



HAL
open science

The CELL NUMBER REGULATOR FW2.2 protein regulates cell-to-cell communication in tomato by modulating callose deposition at plasmodesmata

Arthur Beauchet, Norbert Bollier, Magali Grison, Valérie Rofidal, Frédéric Gévaudant, Emmanuelle M F Bayer, Nathalie Gonzalez, Christian Chevalier

► To cite this version:

Arthur Beauchet, Norbert Bollier, Magali Grison, Valérie Rofidal, Frédéric Gévaudant, et al.. The CELL NUMBER REGULATOR FW2.2 protein regulates cell-to-cell communication in tomato by modulating callose deposition at plasmodesmata. *Plant Physiology*, 2024, 10.1093/plphys/kiae198 . hal-04542052v2

HAL Id: hal-04542052

<https://hal.inrae.fr/hal-04542052v2>

Submitted on 14 Jun 2024

HAL is a multi-disciplinary open access archive for the deposit and dissemination of scientific research documents, whether they are published or not. The documents may come from teaching and research institutions in France or abroad, or from public or private research centers.

L'archive ouverte pluridisciplinaire **HAL**, est destinée au dépôt et à la diffusion de documents scientifiques de niveau recherche, publiés ou non, émanant des établissements d'enseignement et de recherche français ou étrangers, des laboratoires publics ou privés.



Distributed under a Creative Commons Attribution - NonCommercial - NoDerivatives 4.0 International License

The CELL NUMBER REGULATOR FW2.2 protein regulates cell-to-cell communication in tomato by modulating callose deposition at plasmodesmata

Arthur Beauchet ^{1,†,‡} Norbert Bollier ^{1,†} Magali Grison ² Valérie Rofidal ³ Frédéric Gévaudant ¹
Emmanuelle Bayer ² Nathalie Gonzalez ^{1,*} Christian Chevalier ^{1,*}

¹ INRAE, UMR1332 Biologie du Fruit et Pathologie, Université Bordeaux, Villenave d'Ornon F-33140, France

² CNRS, UMR5200 Laboratoire de Biogenèse Membranaire, Université Bordeaux, Villenave d'Ornon F-33140, France

³ IPSiM, CNRS, INRAE, Institut Sup Agro, Université Montpellier, Montpellier F-34060, France

*Author for correspondence: nathalie.gonzalez@inrae.fr (N.G.), christian.chevalier@inrae.fr (C.C.)

[†]A.B. and N.B. contributed equally to this work.

[‡]Present address: VIB-UGent for Plant Systems Biology, Ghent University, Ghent 9052, Belgium.

The authors responsible for distribution of materials integral to the findings presented in this article in accordance with the policy described in the Instructions for Authors (<https://academic.oup.com/plphys/pages/General-Instructions>) are: Nathalie Gonzalez (nathalie.gonzalez@inrae.fr) and Christian Chevalier (christian.chevalier@inrae.fr).

Abstract

FW2.2 (standing for *FRUIT WEIGHT 2.2*), the founding member of the *CELL NUMBER REGULATOR* (*CNR*) gene family, was the first cloned gene underlying a quantitative trait locus (QTL) governing fruit size and weight in tomato (*Solanum lycopersicum*). However, despite this discovery over 20 yr ago, the molecular mechanisms by which FW2.2 negatively regulates cell division during fruit growth remain undeciphered. In the present study, we confirmed that FW2.2 is a membrane-anchored protein whose N- and C-terminal ends face the apoplast. We unexpectedly found that FW2.2 is located at plasmodesmata (PD). FW2.2 participates in the spatiotemporal regulation of callose deposition at PD and belongs to a protein complex which encompasses callose synthases. These results suggest that FW2.2 has a regulatory role in cell-to-cell communication by modulating PD transport capacity and trafficking of signaling molecules during fruit development.

Introduction

The tight coordination of developmental processes such as cell division, cell expansion, and cell differentiation is pivotal for proper plant growth at the whole organismal, organ, and tissue level. Unraveling the genes that contribute to impact plant yield and biomass, and improve agronomic quality traits, is thus a major goal of plant biology and agronomy. In the particular case of tomato (*Solanum lycopersicum*) fruit size determination, nearly 30 quantitative trait loci (QTLs) governing fruit size/weight have been identified (Grandillo

et al. 1999; Lippman and Tanksley 2001; van der Knaap and Tanksley 2003). However, the molecular basis governing these QTLs remains mostly undeciphered, and only 3 major genes underlying such QTLs in tomato have been identified and cloned so far (Frery et al. 2000; Chakrabarti et al. 2013; Mu et al. 2017).

FW2.2 (standing for Fruit Weight QTL on chromosome 2, number 2; Solyc02g090730) was the first cloned gene underlying a QTL related to fruit size in tomato (Alpert et al. 1995; Frery et al. 2000). The encoded protein FW2.2 was defined as

Received September 27, 2023. Accepted February 28, 2024. Advance access publication April 8, 2024.

© The Author(s) 2024. Published by Oxford University Press on behalf of American Society of Plant Biologists.

This is an Open Access article distributed under the terms of the Creative Commons Attribution-NonCommercial-NoDerivs licence (<https://creativecommons.org/licenses/by-nc-nd/4.0/>), which permits non-commercial reproduction and distribution of the work, in any medium, provided the original work is not altered or transformed in any way, and that the work is properly cited. For commercial re-use, please contact reprints@oup.com for reprints and translation rights for reprints. All other permissions can be obtained through our RightsLink service via the Permissions link on the article page on our site—for further information please contact journals.permissions@oup.com.

Open Access

a major negative regulator of cell divisions in young developing fruit, thus impacting fruit size (Frary et al. 2000; Nesbitt and Tanksley 2001; Cong et al. 2002; Liu et al. 2003; Baldet et al. 2006). FW2.2 was the founding member of the CELL NUMBER REGULATOR/FW2.2-Like (CNR/FWL) protein family (Guo et al. 2010), whose function in organ size control seems to be conserved in both monocotyledon and dicotyledon plants (for a review, see Beauchet et al. 2021). Members of this protein family possess a conserved PLAC8 (Placenta-specific gene 8 protein) domain (Galaviz-Hernandez et al. 2003), which is composed of 1 or 2 hydrophobic segments, predicted to form transmembrane (TM) helices (Song et al. 2004). The hydrophobic segments are characterized by the presence of conserved Cys-rich motifs of the type CLXXXCPC or CCXXXCPC, separated by a variable region and located at the N-terminal part of a first TM domain (Beauchet et al. 2021). A localization at the plasma membrane (PM) was indeed demonstrated for the tomato FW2.2 protein (Cong and Tanksley 2006), as well as for CNR/FWL homologous proteins in various fruit species such as eggplant (*Solanum melongena*), pepper (*Capsicum annuum*), *Physalis* (*Physalis floridana*), avocado (*Persea americana*), cherry (*Prunus cerasus*) (Dahan et al. 2010; De Franceschi et al. 2013; Doganlar et al. 2002; Li and He 2015), but also in *Arabidopsis* (*Arabidopsis thaliana*), cereal, and leguminous species (Guo et al. 2010; Libault et al. 2010; Song et al. 2010; Xu et al. 2013). In soybean (*Glycine max*), the CNR/FWL protein GmFWL1 (*Glycine max* FW2.2-Like 1) was shown to display a punctate localization in plasma membrane nanodomains, which supported its ability to interact with membrane nanodomain-associated proteins such as flotillins, prohibitins, remorins, proton- and vacuolar-ATPases, receptor kinases, and leucine-rich repeat proteins (Qiao et al. 2017).

Despite the seemingly conserved roles in cell division and organ size control (Beauchet et al. 2021), the precise physiological and biochemical function of FW2.2 or its CNR/FWL homologs remains unknown so far. The conceptual question in studying the functional role of FW2.2 and CNR/FWL is thus how to conciliate a localization at the plasma membrane and nanodomains with a spatial and temporal control of cell divisions in order to regulate plant organ growth.

In plants, important biological functions are associated to membrane nanodomains, such as cell-to-cell communication occurring at plasmodesmata (PD). PD are cell wall- and membrane-spanning channels, which provide direct cytosolic continuity to mediate symplastic communication between cells (Maule et al. 2011; Petit et al. 2020). PD control cell-to-cell movements of different mobile signaling molecules (Van Norman et al. 2011; Gallagher et al. 2014), and thus regulate the connection between cells ensuring both local and systemic responses to biotic and abiotic stresses, the exchange of nutrients and organs, regulating symbiotic interactions and supporting the coordination of developmental processes (Han et al. 2014a; Gaudioso-Pedraza et al. 2018; O'Lexy et al. 2018; Grison et al. 2019; Yan et al. 2019).

Hormones, metabolites, non-cell autonomous proteins, including transcription factors (TFs), and small RNAs represent such mobile signaling molecules, trafficking from cell to cell via PD. The symplastic communication via PD is finely tuned by developmental or environmental factors, which exert a control on the size exclusion limit of PD. Among these factors, the deposition of callose, a (1,3)- β -glucan polymer, regulated by the antagonistic action of callose synthases and β -glucanases, is a major process that constricts the PD channel, and thus decreases the aperture of PD (Amsbury et al. 2018). Consequently, the balance between callose deposition and degradation at the neck region of PD plays a major role in the regulation of cell-to-cell communication.

In an effort to unravel the cellular and molecular mechanisms sustaining the mode of action of FW2.2 in tomato, we re-investigated its subcellular localization in planta. We unexpectedly found that FW2.2 protein not only associates with bulk PM but also clusters at PD in the different tissues we examined. We further show that FW2.2 modulates the functionality of PD by modifying callose levels. FW2.2-induced regulation of callose most likely occurs through an interaction with PD-associated Callose Synthases. Our data shed light on an unforeseen function of FW2.2 in modulating cell-to-cell communication in tomato.

Results

FW2.2 localizes at the plasma membrane with the N- and C-terminal parts facing the apoplast

The first and only demonstration that FW2.2 addresses the PM was provided by transient expression analysis using onion (*Allium cepa*) epidermal cells and tomato young leaf cells (Cong and Tanksley 2006). This PM localization was described at the time as being conferred by 2 predicted transmembrane domains (TMDs) contained in the PLAC8 domain, but the exact topology of the FW2.2 protein at PM is still uncharacterized.

First, we confirmed the PM localization of FW2.2, using transient expression in *Nicotiana benthamiana* leaves. FW2.2 fused to GFP either at its C-terminus or N-terminus was indeed addressed to the PM (Fig. 1A). The localization at the PM was corroborated after plasmolysis using a 0.4 M mannitol treatment (Supplementary Fig. S1A). We then investigated the topology of FW2.2 at PM by using a Bi-molecular Fluorescent Complementation (BiFC) approach that had been validated for PM-located proteins (Thomas et al. 2008). The FW2.2 protein was fused at its N- or C-terminus to the truncated version of GFP, namely GFP11, which contains the last and eleventh β -sheet. The GFP11-FW2.2 or FW2.2-GFP11 construct was then co-expressed with the cytosolic truncated version of GFP, namely GFP1-10 containing the first 10 β -sheets. Alternatively, the GFP11-FW2.2 or FW2.2-GFP11 construct was co-expressed with a secreted apoplastic version of GFP1-10, namely

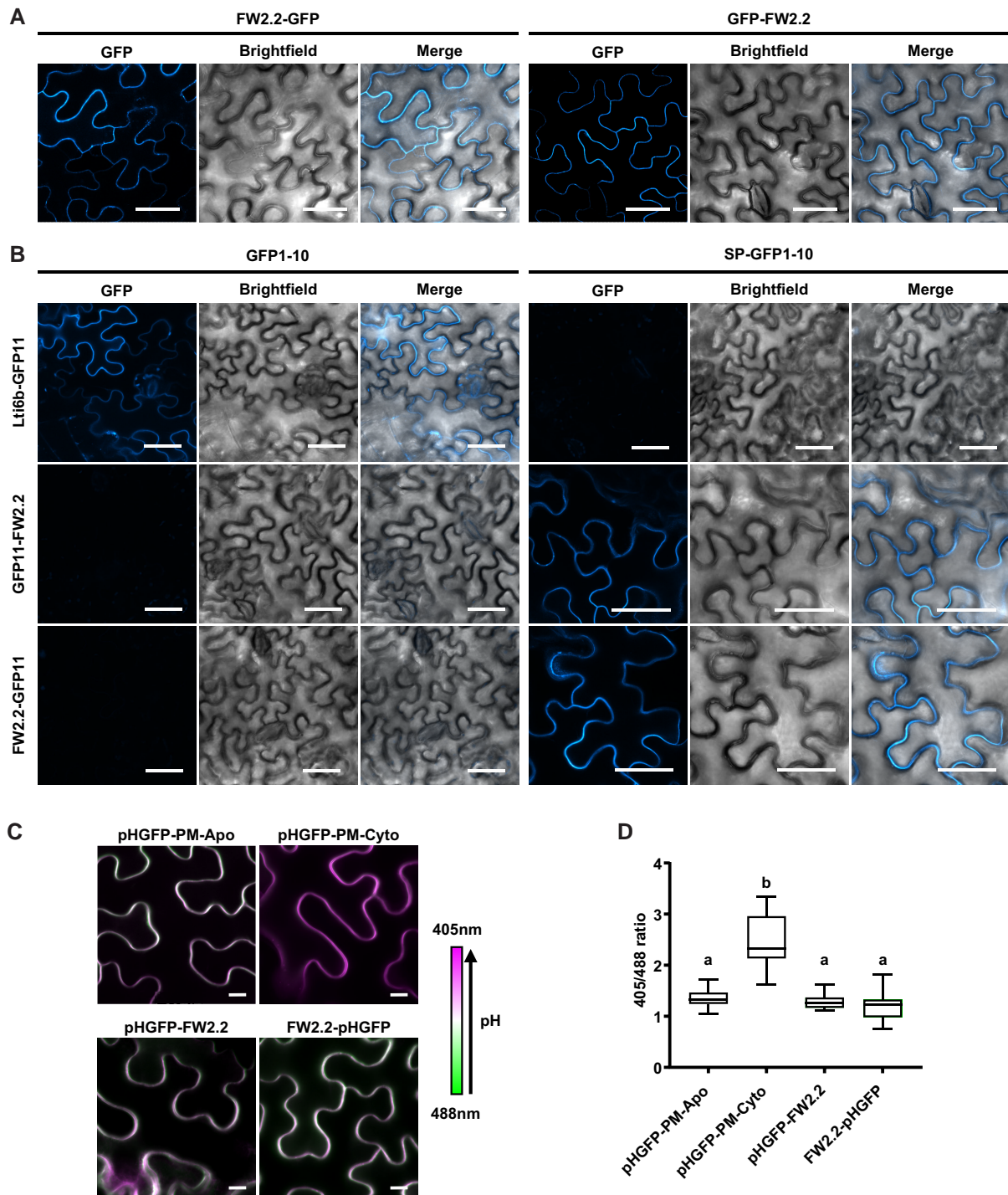


Figure 1. Topological analysis of FW2.2 at the plasma membrane. **A**) Subcellular localization of FW2.2 fused to GFP in *N. benthamiana* leaf epidermal cells. Scale bar = 50 μ m. **B**) BiFC assays deciphering the topology of FW2.2 at the plasma membrane. Transient expressions of FW2.2 or Lti6b fused to GFP11 and with a cytosolic GFP (GFP1-10) or an apoplastic GFP (SP-GFP1-10) were performed in *N. benthamiana* leaves, followed by observation using confocal microscopy. Scale bar = 50 μ m. **C**) Confocal imaging of pHGFP-PM-Apo, pHGFP-PM-Cyto, and pHGFP fused to FW2.2 at the N- and C-termini in *N. benthamiana* leaf epidermal cells. The 4 images were taken using the same confocal settings. Scale bar = 10 μ m. **D**) 405/488 nm intensity ratio at plasma membrane. Boxplot: whiskers extend from minimum to maximum, box extends from the 25th to 75th percentiles, the line in the middle is the median. $n > 15$ different images. ANOVA followed by Tukey's test; $P < 0.05$ between a and b groups.

SP-GFP1-10 (SP for Signal Peptide of the Arabidopsis PR1 protein; At2g14610). As a positive control for a cytosolic interaction, we fused GFP11 to the C-terminal part of the

PM-located protein Lti6b (Low-temperature induced 6b protein; At3g05890) that faces the cytosol (Martinière et al. 2012), and co-infiltrated this construct with GFP1-10. The Lti6b-GFP11

construct was thus expected to be unable to interact with the apoplastic SP-GFP1-10.

A strong GFP signal was observed when the Lti6b-GFP11 was co-expressed with the cytosolic GFP1-10, and no signal was observed when co-expressed with the apoplastic SP-GFP1-10 (Fig. 1B). The co-expression of FW2.2 fused to GFP11 at both its C- and N-termini with the cytosolic GFP1-10 did not result in any visible fluorescence signal. On the contrary, the co-expression of FW2.2 fused to GFP11 with the apoplastic SP-GFP1-10 resulted in a strong GFP signal at the PM (Fig. 1B). Therefore, FW2.2 is associated to PM as previously reported (Cong and Tanksley 2006), and we here provided evidence that the N- and C-termini are facing the apoplast.

To confirm this topology, we performed a second transient expression assay, using a system of apoplastic and cytoplasmic pH sensors described by Martinière et al. (2018) (Fig. 1C). This system takes advantage of the pH-sensitive ratiometric behavior of the protein pHluorin (pHGFP), whose emitted fluorescence differs according to its location in the cytosol or the apoplast, depending on their respective pH value of ~ 7.5 or ~ 6.0 . Following agro-infiltration of *N. benthamiana* leaves, the fluorescence emitted by pHGFP was recorded after an excitation wavelength of 405 and 488 nm, to establish a 405/488 fluorescence intensity ratio, indicative of pH differences. The discrimination between the apoplastic and cytosolic 405/488 ratio was made possible by the use of the following constructs. The apoplastic membrane pH sensor pHGFP-PM-Apo resulted from the fusion of pHGFP with the TMD of the PM-localized protein TM23 (Brandizzi et al. 2002), and the cytosolic membrane pH sensor pHGFP-PM-Cyto corresponded to the fusion of pHGFP with the C-terminal farnesylation sequence of Ras which is anchored to the PM (Martinière et al. 2018).

As expected, the 405/488 nm fluorescence ratio measured in *N. benthamiana* cells was higher for the pHGFP-PM-Cyto (median = 2.2) when compared to that for pHGFP-PM-Apo (median = 1.3), revealing the higher pH of the cytosolic compartment than that of apoplast (Fig. 1D). The 405/488 nm fluorescence ratio was then measured in cells transformed with FW2.2 fused with the pHGFP either at its N-terminal or C-terminal end. It was shown to be very close to the fluorescence ratio measured with the pHGFP-PM-Apo (median = 1.3), thus demonstrating unequivocally that the N- and C-terminal parts of FW2.2 are facing the apoplast (Fig. 1, C and D).

Interestingly, a 3D model predicting the structure of FW2.2 using the AlphaFold Protein Structure Database (Q9LKV7) confirmed that the N- and C-terminal parts of FW2.2 are folded on the same side of the protein (Supplementary Fig. S1B). In addition, the use of currently available tools for transmembrane topology prediction, such as DeepTMHMM and the PPM web server, indicated that (i) FW2.2 does not cross the plasma membrane as no transmembrane domain can be predicted (Supplementary Fig. S1C), but rather (ii) FW2.2 is anchored in the outer leaflet

of the plasma membrane via its hydrophobic domain encompassing the PLAC8 domain, thus exposing N- and C-terminal termini to the apoplast (Supplementary Fig. S1D).

FW2.2 is enriched at plasmodesmata

To go deeper into the study of the FW2.2 subcellular localization, we generated stable transgenic lines expressing FW2.2 fused to YFP at its C-terminal end under the control of the Cauliflower Mosaic Virus (CaMV) 35S promoter (referred to as 35S::FW2.2-YFP plants), in the cultivated tomato variety 'Ailsa Craig' ('AC'). In these plants, the emitted fluorescence associated to YFP was highly detectable in roots and leaves, and in reproductive organs, namely flowers and fruits (Supplementary Fig. S2A). The localization of FW2.2-YFP at the PM was confirmed in all tissues investigated, namely in roots and fruit pericarp (Fig. 2A), according to a pattern of punctate spots at the cell periphery, suggesting that FW2.2-YFP was enriched at nanodomains as observed previously for the soybean homolog GmFWL1 (Qiao et al. 2017). The same tissue preparations were then stained with aniline blue (AB) to reveal callose deposition, as a marker of PD. The fluorescent dots revealing FW2.2-YFP co-localized with AB staining, at pit field junctions, as shown by the overlapping signal intensity plots (Fig. 2A), thus indicating a localization at PD. It is noteworthy that the localization of FW2.2 at PD was independent from the position of YFP at the C-terminal or N-terminal end of the protein, since we obtained similar results using a 35S::YFP-FW2.2 construct (Supplementary Fig. S2B). The enrichment of FW2.2 at PD was quantified by measuring the plasmodesmata enrichment ratio, named "PD index", corresponding to the FW2.2-YFP fluorescence intensity at PD vs that at the cell periphery, as previously described (Brault et al. 2019; Grison et al. 2019). To measure the PD index in control plants, root and fruit pericarp tissues from WT plants were stained with AB together with FM4.64, a membrane-specific dye (Bolte et al. 2004), as illustrated in Supplementary Fig. S2C. While the PD index in controls was equal to 1 regardless of the tissue tested, a high PD index ranging from 1.7 to 1.9 was measured in root and pericarp cells of 35S::FW2.2-YFP plants, (Fig. 2B), thus demonstrating that FW2.2 was enriched at PD.

The overexpression of FW2.2 in leaves enhances cell-to-cell diffusion capacity

Since FW2.2 localizes at PD, we hypothesized that it could contribute to a function associated to cell-to-cell communication. To test this hypothesis, a new set of gain-of-function plants were generated in the tomato cultivar 'AC', as to overexpress FW2.2 constitutively and ectopically, under the control of the 35S promoter (referred to as 35S::FW2.2). Three lines were selected with medium- (2-fold more) to very high levels (50-fold more) of FW2.2 overexpression in 5 days-post-anthesis (DPA) fruits, a stage when the endogenous FW2.2 expression is at its maximum (Supplementary Fig. S3A). In parallel, loss-of-function plants were generated

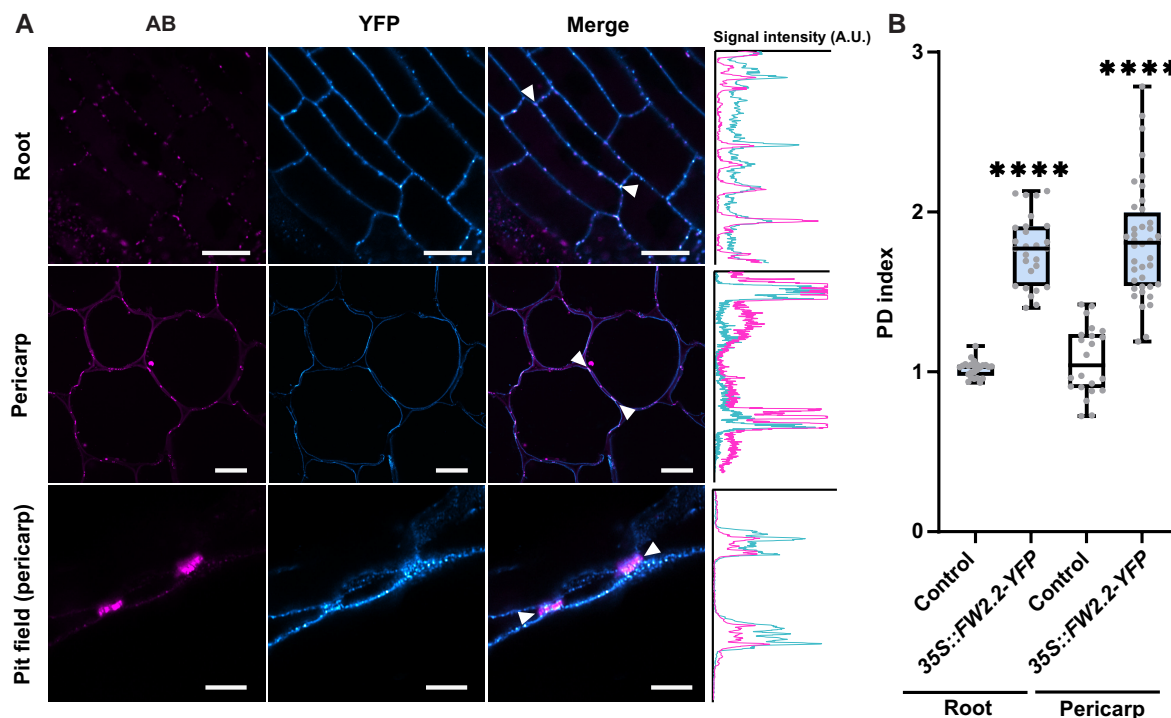


Figure 2. FW2.2 is enriched at PD. **A**) Confocal microscope observations of FW2.2-YFP localization in roots, pericarp, and pit field junctions in pericarp cells from 35S::FW2.2-YFP plants. Scale bar = 10 μ m (root and pericarp); =5 μ m (pit field). Intensity plots delineated by the 2 arrowheads are shown for each co-localization pattern. A.U., arbitrary unit. **B**) PD index for FW2.2 in roots and pericarp tissue of 35S::FW2.2-YFP plants compared to WT. Boxplot: whiskers extend from minimum to maximum, box extends from the 25th to 75th percentiles, the line in the middle is the median. $n > 20$ ROIs from 5 images. Statistical analysis: Student's *t*-test. **** $P < 0.0001$.

using the CRISPR/Cas9 technology. To knock out *FW2.2*, 2 single-guide RNAs (sgRNAs) were designed as close as possible to the start codon of the coding sequence to create a frameshift or an early stop codon resulting in a dysfunctional FW2.2 protein in which the PLAC8 domain is missing (Supplementary Fig. S4). We selected 3 different homozygous lines, referred to as *CR-fw2.2* hereafter.

In all 3 independent 35S::FW2.2 overexpressing lines, a significant reduction in mean leaf surface was observed, from 33% to 42% compared to that in WT (Fig. 3A). This reduction in leaf surface was not due to any alteration in cell size, as the leaf epidermal cell density, used as a proxy for cell size, was unaffected (Fig. 3B). No growth-related phenotype was observed in leaves of *CR-fw2.2* plants, which was expected as FW2.2 is not naturally expressed in leaves (Supplementary Fig. S3B).

We next investigated whether the overexpression of FW2.2 in leaves could affect the permeability of PD, and consequently the cell-to-cell communication. The PD permeability in WT, 35S::FW2.2, and *CR-fw2.2* lines was compared by performing “Drop-ANd-See” (DANS) quantitative assays (Cui et al. 2015), using the membrane-permeable, nonfluorescent dye Carboxy-Fluorescein DiAcetate (CFDA). DANS assays are based on the ability of cells to uptake CFDA rapidly; intracellular esterases then cleave CFDA into fluorescent but membrane-impermeable Carboxy-Fluorescein (CF), and CF diffuses symplastically into the neighboring cells only via

PD. To our knowledge, the use of this technique has never been reported in tomato. We first checked that DANS assays are functional in tomato using leaflets of 4-wk-old plants (Supplementary Fig. S5A).

In Arabidopsis, a pretreatment with 10 mM H₂O₂ alters PD permeability through an increase in callose deposition (Cui and Lee 2016). Such an effect was also observed in tomato WT leaves, as revealed by the reduction in CF-foci area compared to mock-treated leaves, thus indicating a decrease in PD permeability affecting the cell-to-cell movement of CF in tomato leaves (Fig. 3, C and D). We then examined whether gain- or loss-of-function of FW2.2 alters cell-to-cell communication. The CF-foci area was increased (from 20% to 30%) in all overexpressing 35S::FW2.2 lines compared to that in WT, suggesting an increased PD permeability (Fig. 3, C and D). Interestingly, the H₂O₂ treatment which increases callose deposition in WT and thereby decreases PD permeability had no effect on the 35S::FW2.2 lines, compared to the mock treatment. Hence, not only the overexpression of FW2.2 in leaves increased PD permeability but it also inhibited the negative effects of H₂O₂ on it. On the contrary, the CF-foci area in *CR-fw2.2* lines was similar to that in WT (Fig. 3, C and D), showing no difference in CF diffusion, which suggests that the PD permeability was not affected. This absence of effects on PD permeability in *CR-fw2.2* lines can be explained by the absence of endogenous FW2.2 expression in leaves, as mentioned above. It also corroborates with the

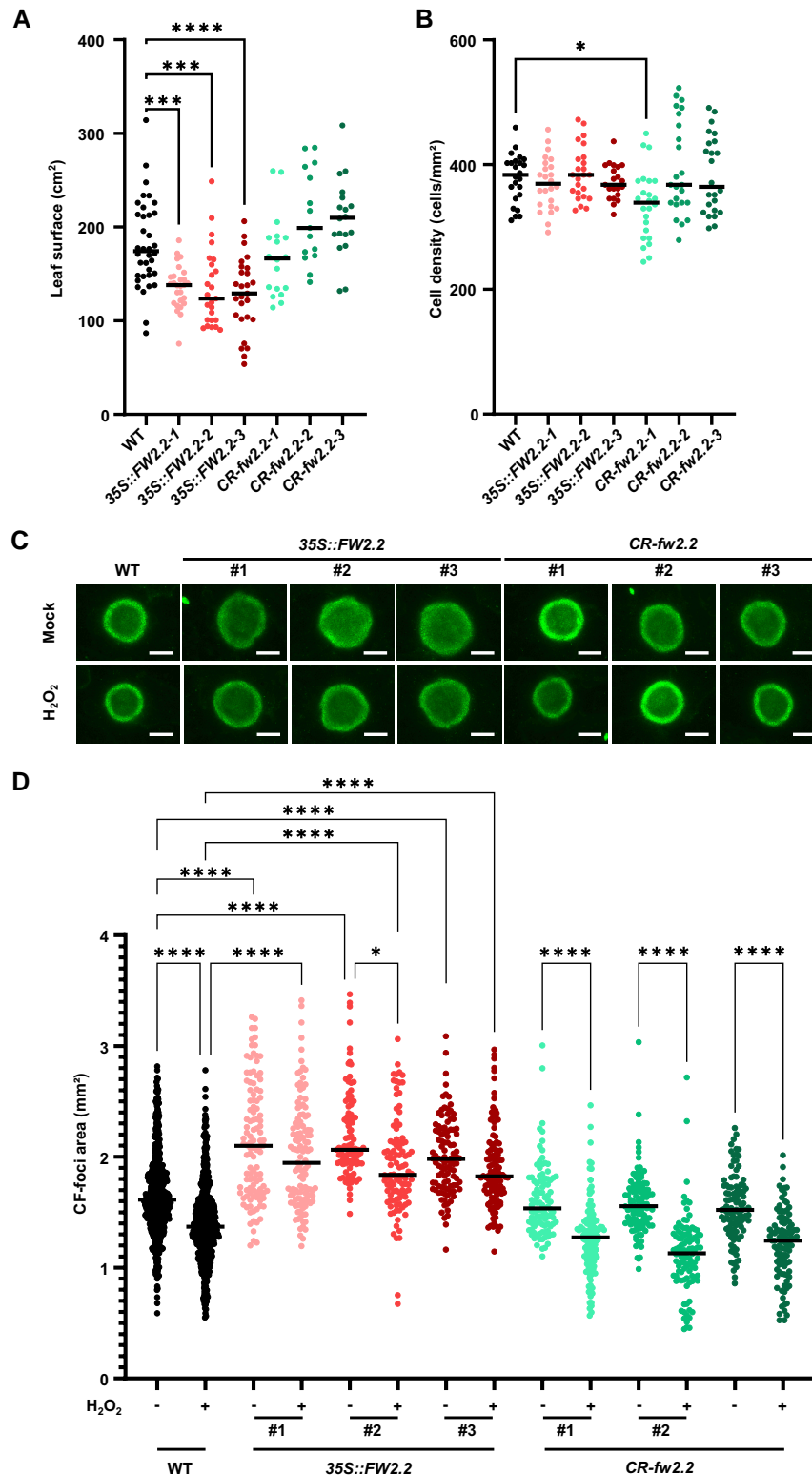


Figure 3. The overexpression of *FW2.2* enhances cell-to-cell diffusion in leaves. **A**) Determination of the mean mature leaf surface in WT, 35S::*FW2.2*, and *CR-fw2.2* lines. $n > 15$ leaves from 5 plants per genotype (each dot represents 1 leaf surface measurement). **B**) Determination of the cell density in leaves from WT, 35S::*FW2.2*, and *CR-fw2.2* lines. $n > 24$ images from 3 plants per genotype (each dot represents 1 measurement of the number cells per mm²). **C**) DANS assays using leaves from WT, 35S::*FW2.2*, and *CR-fw2.2* lines with or without H₂O₂ treatment. Scale bar = 500 μ m. **D**) Quantification of the CF-foci area in WT, 35S::*FW2.2*, and *CR-fw2.2* lines with or without H₂O₂ treatment. Statistical analysis: Kruskal–Wallis test with post hoc Dunn multiple comparison test. * $P < 0.05$; *** $P < 0.001$; **** $P < 0.0001$. $n > 100$ CF-foci from >20 different leaflets from ≥ 6 plants per genotype (each dot represents the measurement of individual foci area).

(Grison et al. 2019; Platre et al. 2022; Wang et al. 2023). Compared to control conditions (mock treatment), the signal intensity for callose in WT leaves treated with H₂O₂ was increased, in agreement with DANS assays showing decreased cell-cell communication. The immunofluorescence intensity in the 35S::FW2.2 leaves was decreased when compared to that in WT, indicating that less callose was deposited, in the absence of any alteration in cell size and leaf thickness as verified before (Fig. 3B and Supplementary Fig. S5B). In response to H₂O₂, the levels of callose deposition in 35S::FW2.2 leaves also increased, but to a much lower extent than in WT (Fig. 4B). On the contrary, the levels of callose deposition in CR-*fw2.2* leaves with or without H₂O₂ were highly similar to that in WT, in accordance with the absence of phenotype when FW2.2 is mutated (Fig. 3). These results clearly indicated that FW2.2 alters the process of callose deposition at PD.

FW2.2 regulates negatively callose deposition at PD in fruit pericarp

Since FW2.2 was found as a major regulator of fruit weight, we next examined whether the misexpression of FW2.2 would affect the level of callose deposition at PD in fruit pericarp tissue.

At a macroscopic level, among the 3 selected overexpressing lines, a significant reduction in mean fruit weight was observed for the 35S::FW2.2-1 and 35S::FW2.2-3 lines (according to an average decrease of 19.6% and 11.3%, respectively) (Fig. 5A). The mean fruit weight in the 3 CR-*fw2.2* loss-of-function plants was higher than that of the WT (7.2%, 7.1%, and 6.3%, respectively). However, these differences were not statistically significant, because of a high variability in fruit weight values. In addition, there was no modification in pericarp thickness in mature fruits from the three 35S::FW2.2 lines compared to WT fruits, while pericarp from CR-*fw2.2* fruits appeared thinner (Fig. 5B). Related to fruit structure, fruits from gain- and loss-of-function plants were all affected for the number of locules to various degrees (Fig. 5C). More fruits with less than 3 locules were encountered in the overexpressing 35S::FW2.2 lines, while fruits with 4 and even more locules were observed in CR-*fw2.2* lines, compared to WT fruits from the 'AC' cultivar which usually contain 3 locules. This converse impact on the number of fruit locules in the gain- and loss-of-function plants suggests that cell divisions have been impacted in the floral meristem (FM) termination process, through the increased or repressed negative regulatory effect in 35S::FW2.2 or CR-*fw2.2* lines, respectively.

The level of callose deposition was then investigated on pericarp sections of fruits from the 35S::FW2.2 and CR-*fw2.2* plants harvested at 5 and 15 DPA. These 2 different developmental stages were chosen because FW2.2 is highly expressed in the pericarp of 5 DPA fruit and much less at 15 DPA (Supplementary Fig. S3B). At both 5 and 15 DPA, the immunofluorescence signal intensity in the pericarp of

35S::FW2.2 fruits was decreased when compared to that in WT, indicating that the level of callose deposition was reduced (Fig. 5, E and F and Supplementary Fig. S7). On the contrary, the immunofluorescence signal intensity in the pericarp of CR-*fw2.2* fruits at 5 DPA was increased significantly when compared to that in WT, thus revealing a higher level of callose deposition. Interestingly, except for a slight significant increase in the CR-*fw2.2-3* line, no increase in callose deposition was observed at 15 DPA in pericarp sections from CR-*fw2.2* fruits compared to WT. This can be explained by the very low expression of FW2.2 in 15 DPA fruits (Supplementary Fig. S3B), and thus the absence of any loss-of-function effect from the CRISPR-Cas9 construct on FW2.2 at this developmental stage.

Cell perimeters were measured for all genotypes in all the different cell layers composing the fruit pericarp at 5 DPA, and in the mesocarp at 15 DPA, to ascertain that these differences in callose deposition was not due to any heterogeneity in cell size, and thus in the density of cell walls. The cell perimeter was comparable in all WT, 35S::FW2.2, and CR-*fw2.2* lines, with only slightly smaller values in some cases, especially in the internal part of the mesocarp (Supplementary Fig. S8). Hence, the observed differences in callose deposition did originate from the effects of FW2.2 gain- and loss-of-function, demonstrating that FW2.2 regulates negatively the process of callose deposition at PD within fruit pericarp.

FW2.2 pull-down reveals plasmodesmata-related proteins

To go deeper into the functional and biochemical characterization of FW2.2, an *in vivo* approach using immunoprecipitation followed by tandem-mass spectrometry (IP-MS/MS) was performed to identify interacting protein partners of FW2.2 inside the pericarp from 35S::FW2.2-YFP fruits harvested at 10 DPA. Since FW2.2 is still expressed endogenously at this developmental stage, it was therefore expected that its natural interacting proteins would be present in the protein extracts. The IP-MS/MS experiment resulted in the identification of 662 proteins that co-immunoprecipitated with FW2.2, which were enriched in the 35S::FW2.2-YFP sample when compared to WT (Fig. 6A, Supplementary Data Set 1). To identify potential PD-localized candidates in relation with FW2.2 function, we compared this list with a tentative PD proteome from tomato made of a total of 400 proteins corresponding to the deduced orthologs of the 115 proteins constituting the refined PD proteome from Arabidopsis published by Brault et al. (2019). Seventeen proteins were found overlapping between the 2 proteomes (Fig. 6B). Three distinct classes of proteins, all key regulators of cell-to-cell signaling in plants, represented almost 2/3 of the identified proteins (Fig. 6C): (i) 2 proteins of the C2 calcium/lipid-binding phosphoribosyl transferase family (Solyc01g080430 and Solyc01g094410), belonging to the large family of multiple C2 domains and transmembrane region proteins

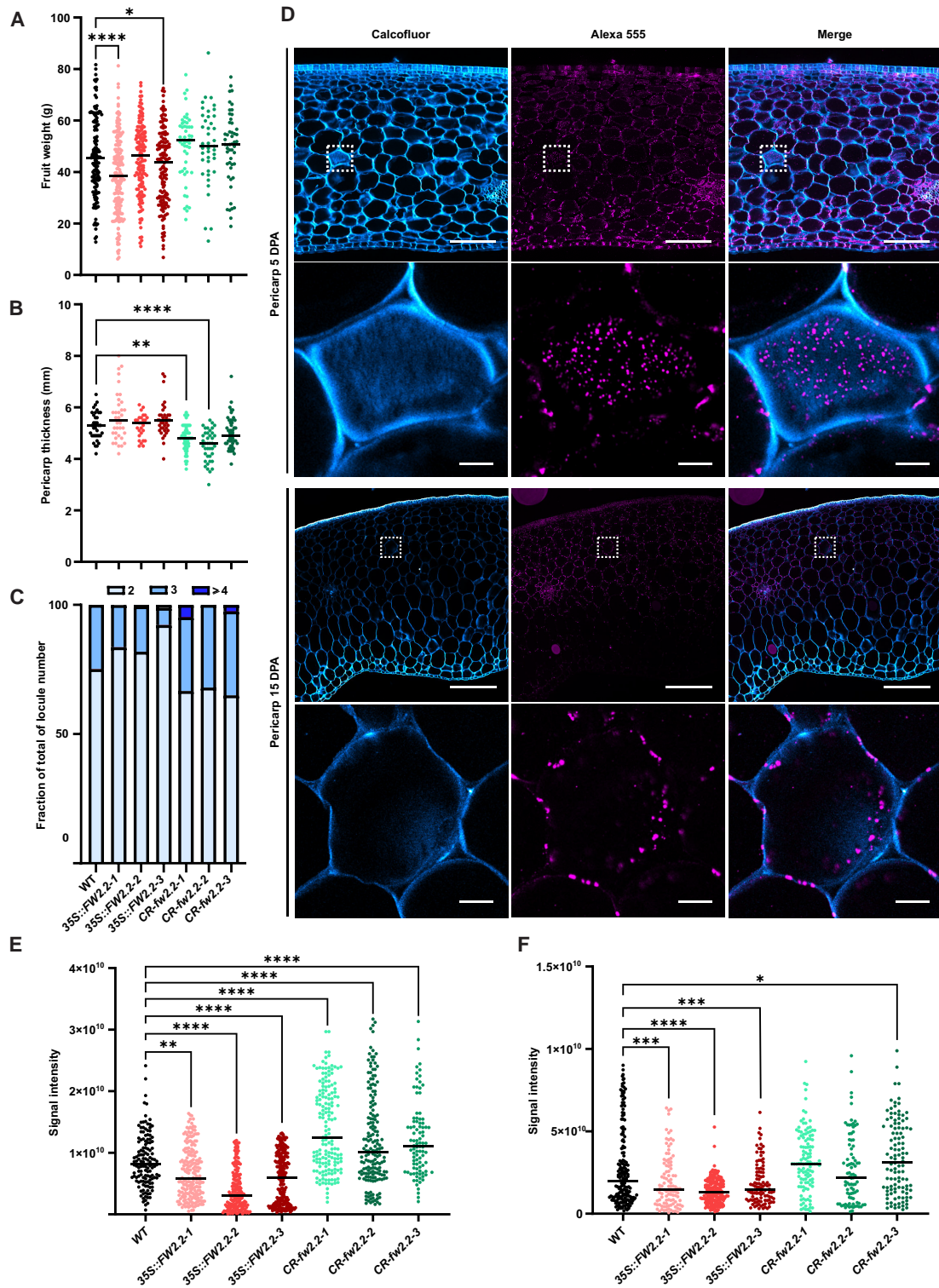


Figure 5. Callose deposition is altered at 5 and 15 DPA in fruit pericarp of 35S::FW2.2 and CR-fw2.2 plants. **A to C**) Phenotypic analysis of fruits (at breaker stage) from 35S::FW2.2 and CR-fw2.2 plants compared to that of WT: determination of the mean fruit weight **A**), $n > 40$ fruits from 4 plants per line; determination of the pericarp thickness **B**); determination of the number of fruit locules **C**), $n > 25$ fruits from 4 plants per lines. **D**) Immunolabeling of callose in 5 DPA (top) and 15 DPA (bottom) pericarp from WT fruits. Scale bar = 100 μ m (5 DPA); =500 μ m (15 DPA); =25 μ m (15 DPA close-up). **E, F**) Level of callose deposition in WT, 35S::FW2.2, and CR-fw2.2 lines at 5 **E**) and 15 DPA **F**). The signal intensity for callose deposition is integrated to the pixel surface measured. Statistical analysis applied to all panels (**A to F**) was as follows: Kruskal–Wallis test with post hoc Dunn multiple comparison test. * $P < 0.05$; ** $P < 0.01$; *** $P < 0.001$; **** $P < 0.0001$. $n > 80$ images measurement from 4 to 5 pericarp slices of 4 to 5 fruits for each line.

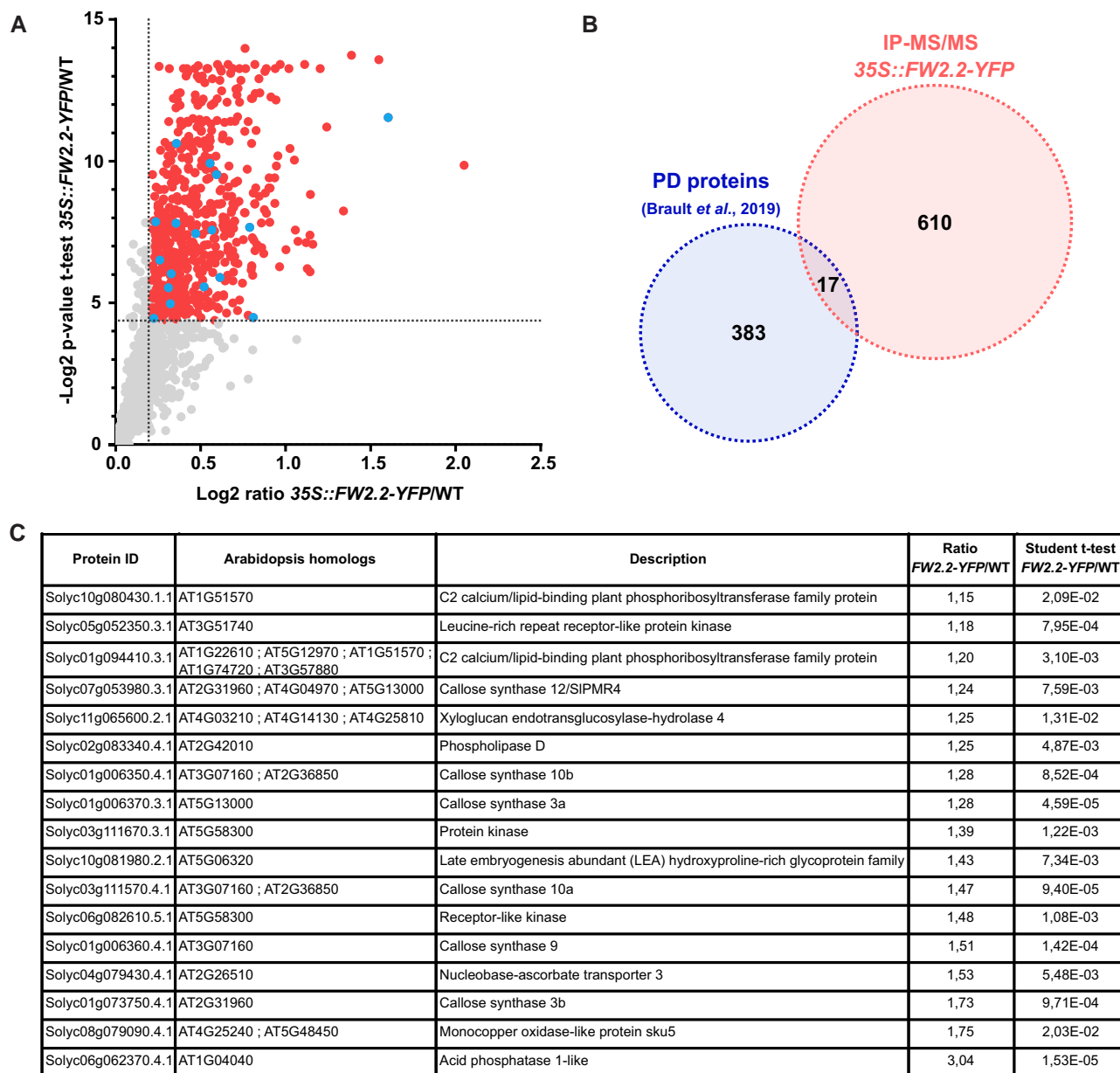


Figure 6. FW2.2 co-immunoprecipitates with several PD-localized proteins including callose synthases. **A)** Dot plots showing enriched proteins in 35S::FW2.2-YFP IP-MS/MS experiments in 10 DPA pericarp. Red dot indicates significantly enriched protein (based on a Student's *t*-test with Benjamini–Hochberg correction $P < 0.05$ and an enrichment ratio > 1.15). Blue dots indicate proteins found in the PD proteome. **B)** Venn diagram showing the overlap between the IP-MS/MS proteome and the PD proteome from Brault et al. (2019). Statistical analysis: hypergeometric test $P = 0.0021$. **C)** List of plasmodesmata associated proteins detected in the IP-MS/MS proteome.

(MCTP) (Brault et al. 2019); (ii) 3 proteins of Leucine-Rich Repeat Receptor-Like kinases (LRR-RLKs) family (Solyc03g111670, Solyc06g082610, and Solyc05g052350) (Wei et al. 2015); and (iii) 6 different Callose Synthases (CalS), which were identified based on their phylogenetic proximity to Arabidopsis counterparts, namely SICalS1 (Solyc01g006350), SICalS3a (Solyc01g006370), SICalS3b (Solyc01g073750), SICalS9 (Solyc01g006360), SICalS10a (Solyc03g111570), and SICalS12 (Solyc07g053980) (Supplementary Fig. S9A). The co-immunoprecipitation of FW2.2 with Callose synthases in 10 DPA fruits was thus

fully relevant with its aforementioned role in regulating callose deposition at PD in the pericarp. RT-qPCR analyses confirmed that these 6 *CalS* genes were expressed in WT fruit pericarp at 10 DPA (Supplementary Fig. S9B), and no significant change in their expression level occurred in the FW2.2 loss- and gain-of-function plants (Supplementary Fig. S10).

These results indicate that FW2.2 belongs to a protein complex at PD which includes Callose Synthases, and thus support the functional role of FW2.2 on PD permeability and cell-to-cell communication.

Discussion

FW2.2 was the first gene underlying a QTL related to fruit size to be cloned in tomato (Frery et al. 2000). It is by far the major QTL of such type, as it accounts for as much as a 30% difference in fruit fresh weight between domesticated (large-fruited) tomatoes and their wild (small-fruited) relatives (Grandillo et al. 1999; Frery et al. 2000). Most wild-small fruited-tomatoes (if not all) possess “small-fruit” alleles; conversely all domesticated/cultivated-large fruited-tomatoes possess “large-fruit” alleles (Blanca et al. 2015). Comparative sequence analysis of FW2.2 from the large- and small-fruited alleles indicated that the FW2.2 effects on fruit size do not originate from differences in the sequence and structure of the protein, but rather from the timing of its transcription (heterochronic changes) and the overall quantity of transcripts in the fruit (Cong et al. 2002). The “large-fruit” allele is rapidly transcribed to reach a peak of expression around 5 DPA, whereas the “small-fruit” allele is transcribed more slowly and displays its maximum of expression nearly a week later (12 to 15 DPA), reaching almost twice the mRNA level observed in large-fruit allele (Cong et al. 2002). Since this difference in timing of expression was found inversely associated to the mitotic activity, FW2.2 was defined as a negative regulator of cell divisions in pre-anthesis ovary and developing fruit, thus modulating final fruit size (Frery et al. 2000; Cong et al. 2002). Such a function in regulating organ size by modulating cell number was found conserved for many other plant homologs of FW2.2 (Beauchet et al. 2021), which led to the attribution of the CELL NUMBER REGULATOR (CNR) protein family name (Guo et al. 2010). Members of the CNR protein family are targeted to the PM, due to the presence of the PLAC8 domain (Beauchet et al. 2021). However, the precise biological function and mechanism of action of membrane-embedded FW2.2 and CNRs in controlling organ size via the regulation of cell divisions remained totally elusive so far.

FW2.2 regulates cell-to-cell diffusion by modulating callose deposition at plasmodesmata

It was long known that FW2.2 is a plasma membrane-located protein (Cong and Tanksley 2006). Using transient expression in *N. benthamiana* leaves and stable transformants in the tomato ‘AC’ cultivar, we confirmed this PM localization for FW2.2 (Figs. 1 and 2). The topology of FW2.2 within the PM was established and revealed that the N- and C-terminal regions are extracellular, thus facing the apoplast (Fig. 1). This is in agreement with a topological model predicted for PfcNR1, the FW2.2 putative orthologue from *P. floridana*, which displays a high degree of identity (80%) with FW2.2 (Li and He 2015). However, our study provides information about the FW2.2 3-D structure and its PM localization. FW2.2 is not a transmembrane protein per se, as no transmembrane domains can be predicted using the current prediction tools, but it is most likely anchored in the outer leaflet of the PM, via the hydrophobic portion of the protein

encompassing the PLAC8 domain (Supplementary Fig. S1). More importantly, we demonstrated unequivocally that FW2.2 is enriched at PD (Fig. 2) and participates in cell-to-cell communication mechanisms via the regulation of PD permeability (Fig. 3).

This localization at PD is most probably functionally conserved with other members of the CNR family. Indeed, the localization of the soybean GmFWL1 protein was described as associated to membrane microdomains (Qiao et al. 2017), according to a punctate pattern very similar to what we observed for FW2.2 in tomato (Fig. 2). It is thus highly probable that GmFWL1 also localizes at PD. The homolog of FW2.2 in Arabidopsis, namely AtPCR2 sharing 44% of identity with FW2.2, belongs to the PD proteome established by Braut et al. (2019), together with well-established PD proteins, and presents a ~50- to 100-fold enrichment at PD compared to the PM, total protein, microsomal, or cell wall fraction.

PD make the connection between adjacent cells to enable the diffusion of mobile signaling molecules (Wu and Gallagher 2011). Using DANS assays, we demonstrated that FW2.2 is involved in cell-to-cell diffusion mechanisms and contributes to increase PD permeability (Fig. 3). The permeability and thus the aperture of PD are mechanically regulated by the extent of deposited callose at the neck of PD (Amsbury et al. 2018). The increase in PD permeability mediated by FW2.2 occurs via a modification in the level of callose deposition, as FW2.2 regulates negatively its accumulation (Figs. 4 and 5). The level of callose deposition is a highly regulated process involving 2 antagonistic enzymes, Callose Synthases and β -1,3-glucanases (Chen and Kim 2009). Callose deposition is enhanced according to 2 main signaling pathways, 1 reactive oxygen species (ROS)-dependent and the other 1 salicylic acid (SA)-dependent, which both induce the expression of receptor proteins such as PDL5 that participate with Callose Synthase proteins in the regulation of PD permeability (Cui and Lee 2016; Amsbury et al. 2018; Tee et al. 2023). The expected decrease in PD permeability under H₂O₂ stress was not observed when FW2.2 is overexpressed, suggesting that FW2.2 play a role in the ROS-dependent pathway. Whether FW2.2 also plays a role in the SA-dependent pathway to regulate PD permeability remains to be determined.

FW2.2 is part of a protein complex involved in plasmodesmata function, which includes Callose Synthases

A proteomics approach using IP-MS/MS revealed that FW2.2 belongs to a protein complex that includes different Callose Synthases: SICaLS1, SICaLS3a, SICaLS3b, SICaLS9, SICaLS10, and SICaLS12 (Fig. 6). Interestingly, all these tomato proteins are the putative orthologs of Arabidopsis CalS known to contribute to callose homeostasis at PD, thereby regulating the permeability of PD and consequently the symplastic molecular exchanges between neighboring cells (Saatian et al. 2023; Usak et al. 2023). It is noteworthy that among the

178 proteins found to interact with GmFWL1, 3 distinct callose synthases, namely CalS5 (Glyma13g31310), CalS8 (Glyma04g36710), and CalS10 (Glyma10g44150), were also identified following the co-immunoprecipitation assays (Qiao et al. 2017). This observation suggests not only that GmFWL1 is probably located at PD as well but also that the interaction between FW2.2 and CNRs with proteins involved in the metabolic process of callose deposition at PD seems to be a conserved feature for the balance between synthesis and degradation of callose at PD. Hence, we can hypothesize that CNRs regulate negatively the activity of Callose Synthases.

The activity of PD-associated Callose Synthases is of prime importance in numerous developmental processes, such as in the response to biotic and abiotic stresses, organ and tissue patterning, cell differentiation, phloem transport, and cell division via the formation of the cell plate at cytokinesis (Amsbury et al. 2018; Wu et al. 2018; Usak et al. 2023). In Arabidopsis, AtCalS1 and AtCalS10 localize at the nascent cell plate where they synthesize callose as the first and fundamental polysaccharide component of the nascent cell plate, and AtCalS9 is essential for the proper commitment to mitosis during male gametogenesis (Usak et al. 2023). Again, putative orthologs for these 3 CalS were found to co-immunoprecipitate with FW2.2 in tomato. Interestingly, the CRR1 protein from rice encodes a CalS which is essential for ovary growth following fertilization (Song et al. 2016). The loss-of-function of CRR1 induces a disordered patterning of vascular cells in the ovaries of the mutant, with aberrant cell wall formation and reduced callose deposition at PD. Furthermore, the cell number inside the *crr1* ovaries is reduced when compared to the WT, establishing a link with callose synthesis and deposition, symplastic pathway via PD and control of cell division during ovary development.

How to reconcile a function of FW2.2 in cell-to-cell communication, cell cycle- and fruit growth regulation?

As FW2.2 was described as a negative regulator of cell division during early fruit development, which ultimately impacts fruit growth (Cong et al. 2002), it would have been expected that a loss-function of FW2.2 results in increased cell divisions and possibly larger organs (including fruits), and conversely that the ectopic overexpression of FW2.2 reduces mitotic activities and results in smaller organs. This latter effect could be observed at least in leaves from 35S::FW2.2 overexpressing lines (Fig. 3), i.e. in organs where FW2.2 is not naturally expressed (Supplementary Fig. S3B). Since the reduction in leaf growth was unrelated to any modification in cell size, this suggests that cell divisions were reduced under the effects of FW2.2 overexpression. In 2 out of 3 gain-of-function lines, we could also observe such a phenotype of reduced size for fruits although limited in extent (Fig. 5).

These results are puzzling since genetics studies showed that the *fw2.2* QTL accounts for 22% to 47% of fruit mass

variation when cultivated tomato cultivars are crossed with the wild species *Solanum pimpinellifolium* or *Solanum pennellii* (Alpert et al. 1995; Lippman and Tanksley 2001; van der Knaap and Tanksley 2003). Nevertheless, the literature is still devoid of any functional characterization of FW2.2 in cultivated tomato plants, albeit the gene was discovered and cloned more than 20 yr ago. This is most probably the result of a lack of phenotypes when FW2.2 is artificially deregulated in transgenic fruits. For instance, Zsögön et al. (2018) aimed at introducing by CRISPR-Cas9 engineering, yield and productivity traits from modern (“large-fruited”) tomato cultivars into the wild (“small-fruited”) tomato *S. pimpinellifolium*. Among the 6 traits studied, these authors selected the FW2.2 locus for fruit weight, and produced several mutants with deletions disrupting FW2.2. However, none of them induced any change in fruit size in T2 lines compared to *S. pimpinellifolium* WT, despite the mutations (Zsögön et al. 2018). These results corroborate the functional analysis reported herein in *S. lycopersicum* cv. ‘AC’, when FW2.2 was mutated in the *CR-fw2.2* loss-of-function plants (Fig. 5). Hence, the ectopic and constitutive expression of FW2.2 driven by the 35S promoter, definitely outside its natural timeframe and territorial regulation, and its loss of function did not impact fruit development significantly, which probably obeys to precise changes in FW2.2 spatiotemporal expression, according to the heterochronic regulation of expression described for the original *fw2.2* mutation (Cong et al. 2002). To cope with this difficulty, we developed an “allele swapping” complementation strategy (Supplementary Fig. S11). This strategy aimed at generating transgenic plants in which the “large-fruit”-allele promoter from *S. lycopersicum* cv. ‘AC’ is used to govern the expression of FW2.2 in a “small-fruit” background, namely the wild tomato *S. pimpinellifolium* (Pi). Conversely, we used the “small-fruit”-allele promoter from *S. pimpinellifolium* to govern the expression of FW2.2 in the “large-fruit” ‘AC’ background. Although we succeeded in the expected allele expression swapping according to the right spatiotemporal expression governed by each of the promoters, we failed to produce any fruit weight phenotypes in the complemented *S. pimpinellifolium* and *S. lycopersicum* cv. ‘AC’ transgenic lines compared to WT plants. Therefore, the effects of FW2.2 on fruit size obey probably to a subtler regulation than the sole quantity of transcripts and availability of the protein. In addition, we cannot exclude that this lack of tangible phenotype may be related to gene redundancy within the CNR/FWL family, as 11 genes homologous to FW2.2 have been reported (Beauchet et al. 2021).

Despite the lack of consistent phenotypes when FW2.2 is misexpressed, the functionality of the protein itself within its cellular and protein environment may be of prime importance. The discovery of the FW2.2 function in cell-to-cell communication via PD thus raises the question of its link with the regulation of cell division, and subsequent fruit size control. By impairing callose deposition and thus maintaining PD aperture, FW2.2 may contribute to facilitate the diffusion of signaling molecules whose nature is still unknown.

As reviewed by Han et al. (2014b), TFs are well characterized examples of such signaling molecules that could play an important part in the determination of fruit size. So far, direct evidences for the symplastic movements via PD of cell cycle regulators have not been reported. However, Weinl et al. (2005) showed that Cyclin-Dependent Kinase (CDK)-specific inhibitors called Kip-Related Proteins (KRPs) can act non-cell-autonomously, as to regulate cell division and growth pattern in leaf epidermis. During tomato fruit development, KRPs are key players in the regulation of cell cycle, and the commitment to endoreduplication, which drives ploidy-dependent fruit growth (Bisbis et al. 2006; Nafati et al. 2011; Tourdot et al. 2023). Whether the negative regulation on cell division exerted by FW2.2 in fruit growth goes through the inactivation of CDK/Cyclin activities via the traffic of KRPs from cell to cell across the pericarp remains an exciting matter of investigation. Recently, Ruan et al. (2020) reported that *OscNR1*, encoded by the underlying gene of a major QTL for grain width and weight in rice, is able to interact with *OskRP1* in the cell membrane. Therefore, this remarkable finding provided evidence of a direct link between a CNR protein controlling organ size and a well-established cell cycle regulator inhibiting cell division. Whether this applies to FW2.2 for the regulation of cell cycle during early fruit development is a challenge for future research as to unravel definitely the function of FW2.2 in the control of fruit size/weight in tomato. Then, the lack of phenotypes observed in our in planta functional analysis may not be only related to the proper spatiotemporal expression of FW2.2 but also to the protein environment itself and the spatiotemporal availability of these putative signaling molecules.

How PD-mediated symplastic signaling affects fruit growth is still poorly understood. By demonstrating that FW2.2 contributes to the spatiotemporal regulation of callose deposition dynamics via regulating the CalS activity, we here provide an important breakthrough for the identification of the molecular and cellular mode of action of FW2.2. Based on our data, we propose a model integrating FW2.2 in the regulation of PD aperture via the dynamics of callose deposition (Fig. 7). We propose that FW2.2 regulates callose deposition, most likely in interaction with a protein complex encompassing Callose synthases, which may modulate negatively their activity, thus ultimately impacting PD permeability and facilitating the cell-to-cell movement of mobile signaling molecules. A future challenge will be to identify the nature of such signaling molecules, which will provide a valuable insight into the molecular mechanisms underlying the complex regulation of organ size, especially fruits.

Materials and methods

Plant materials and growth conditions

Tomato (*S. lycopersicum* cv. 'AC') and *N. benthamiana* plants were grown in soil in a greenhouse under the following

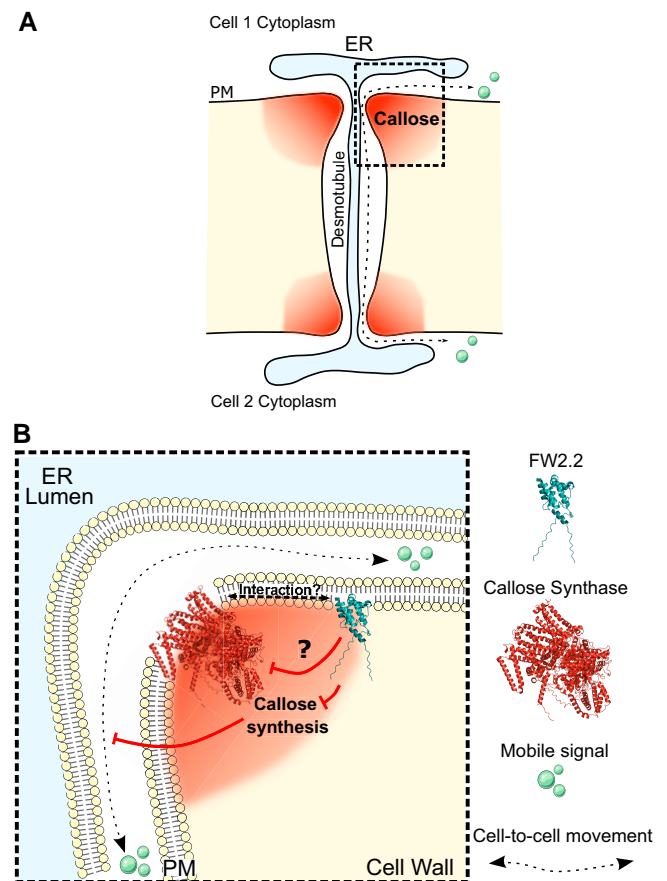


Figure 7. Model illustrating the function of FW2.2 in regulating callose synthesis at PD. **A)** Regulation of PD aperture by callose deposition at the neck region of PD. A high callose deposition level restricts the aperture of PD and the size of signaling molecules passing through. **B)** Molecular and cellular model for the regulation of Callose synthase activity by FW2.2 at PD.

conditions: 16 h day/8 h night cycle, using a set of 100 W warm white LED projectors providing an irradiance of $100 \mu\text{mol m}^{-2} \text{s}^{-1}$ at the level of canopy. The light spectrum was constituted by equivalent levels of blue irradiation (range 430 to 450 nm) and red irradiation (640 to 660 nm). For in vitro culture, tomato seeds were sterilized for 10 min under agitation in a solution of 3.2% (v/v) sodium hypochlorite. Seeds were then washed 3 times with sterile water and dried under a laminar flow hood. Seeds were sowed in Murashige and Skoog medium (1/4 MS) and transferred in a growth chamber under the following conditions: 16 h day/8 h night cycle, 22°C/20°C day/night, using white light (Osram L36 W/77 Fluora 1400 lm) providing 80 to $100 \mu\text{E m}^{-2} \text{s}^{-1}$ intensity light at the stirring plate.

Vector constructs and plant transformation

Vectors for the overexpression of FW2.2 in plants were generated using the Gateway cloning system (Invitrogen, Carlsbad, CA, USA), following manufacturer's instruction.

The *FW2.2* full-length coding sequence was amplified from cDNAs prepared from tomato (cv. 'AC') fruits at 5 DPA using PrimeSTAR MAX DNA polymerase (TAKARA BIO Inc., Kusatsu, Japan) and primers including the attB sites (Supplementary Table S1). The resulting PCR products were cloned into the corresponding Gateway vectors described in Supplementary Table S2. For CRISPR/Cas9 mutagenesis, constructs were assembled using the Golden Gate cloning method (Weber et al. 2011). Two sgRNAs were designed at the 5' end of the coding sequence of *FW2.2* using CRISPOR (Concordet and Haeussler 2018) to generate a premature stop codon (Supplementary Table S1). Primers for creating the sgRNA were designed as follows: tgtggctcaATTG-NNNNNNNN-gtttagtagctagaaatagcaag as a forward primer containing the sgRNA, and tgtggctCAAGCGTAATGCCAACTTTGTAC as a reverse primer. The sequences corresponding to the sgRNA were then PCR amplified using the 2 aforementioned primers, and cloned into the pSLQ1651-sgTelomere plasmid (Addgene #51024). *fw2.2*-sgRNA-1 and *fw2.2*-sgRNA-2 were fused to the Arabidopsis AtU6-26 promoter (Addgene #46968) by digestion-ligation reaction in pICH47751 (Addgene #48002) and pICH47761 (Addgene #48003), respectively. These 2 level 1 vectors were assembled with the Kanamycin resistance gene (pNOS::NPTII-OCST; Addgene #51144), the AtCas9 ($2 \times 35S::AtCAS9$ -OCST; Addgene #112079), and the linker pICH41780 (Addgene #48019) into the level 2 vector pICSL4723 (Kind gift from Dr. Mark Youles, The Sainsbury Laboratory, Norwich, UK). Transgenic plants were generated by *Agrobacterium tumefaciens* (strain C58C1) mediated transformation using explants of tomato cotyledons as described (Swinnen et al. 2022).

RNA extraction and RT-qPCR analysis

Total RNA was isolated from cotyledons, hypocotyls, shoot apical meristems, leaves, roots, flowers, and pericarp tissues from fruits harvested at different developmental stages (5, 10, and 15 DPA), using TRIzol reagent (Invitrogen) in combination with RNeasy Plant Mini Kit (Qiagen) following the manufacturers' instructions. RNase-free DNase (Qiagen) treatment was performed on each sample. Reverse transcription was performed using the iScript cDNA Synthesis Kit (Bio-Rad, Hercules, CA). RT-qPCR was performed using Gotaq qPCR mastermix (Promega, Madison, WI) and a CFX 96 real-time system (Bio-Rad). RT-qPCR primers were designed with PerlPrimer software (Marshall 2004) to overlap 2 exons in order to limit genomic DNA amplification (Supplementary Table S1) and amplify an 80 to 200 bp-long amplicon, with a T_m of 60 °C. The transcript levels of the expressed genes were normalized to that of the housekeeping genes: *SITUBULIN* (Solyc04g081490) in combination with *SINUDK* (Solyc01g089970) for fruit samples, or with *SIEIF4 α* (Solyc12g095990) for other tissue samples, using the $\Delta\Delta CT$ normalization. Data are presented as mean and SD of biological replicates. Statistical significance was evaluated by

the Kruskal–Wallis test and *P*-values are indicated. All primers used for expression analyses are listed in Supplementary Table S1.

Phenotypic characterization

Plants were cultivated randomly side-by-side with WT plants. Flowers were vibrated every day to ensure optimal self-pollination. Seven flowers per inflorescence were maintained to ensure proper development of fruit per inflorescence. Fruits from 4 to 6 plants of each genotype of 2 biological replicates were used to determine fruit weight, fruit size, locule number, and pericarp thickness at the breaker stage of fruit development. Fruits were weighted and measured using a caliper. Then, pictures of equatorial transverse sections of fruits were taken to count the locule number and measure the pericarp thickness, using a Nikon D5300 camera. Image analysis was performed using the ImageJ software (<https://imagej.nih.gov/ij/>). The number of measurements ranged from $n = 50$ to $n = 200$ depending on the number of fruits produced by the different transgenic plants. For leaf surface phenotyping, pictures of full-grown leaves were taken using a Nikon D5300, and analyzed by intensity threshold filtering. To measure the leaf thickness, images of leaf sections acquired for immunolabeling experiments were used with 3 measurement for each picture ($n = 70$ to 100).

PD index determination

The localization of *FW2.2*-YFP at PM and PD was observed using confocal imaging performed on a Zeiss LSM 880 confocal laser scanning microscope equipped with fast AiryScan, using a Zeiss C PL APO x63 oil-immersion objective (numerical aperture 1.4). To ascertain the PM localization of *FW2.2*, *N. benthamiana* leaf cells agro-infiltrated with 35S::*FW2.2*-YFP and fruit pericarp cells from 35S::*FW2.2*-YFP tomato plants were plasmolyzed using 0.4 M mannitol for 15 min before observation. Staining with FM4.64 at a final concentration of 4 μM was used as a control for PM localization (Bolte et al. 2004). For FM4.64 imaging, excitation was performed at 561 nm and fluorescence emission was collected at 630 to 690 nm. For YFP imaging, excitation was performed at 514 nm and fluorescence emission collected at 520 to 580 nm. Staining with aniline blue (AB; Biosupplies, Victoria, Australia) was performed by infiltration of a 0.0125% (w/v) solution; excitation was performed at 405 nm and fluorescence emission collected at 420 to 480 nm. The calculation of PD index was determined by calculating the fluorescence intensity of *FW2.2*-YFP at plasmodesmata and at PM as described (Grison et al. 2019). Images were all acquired with the same parameters (zoom, gain, laser intensity, etc.), and YFP and AB channels were acquired sequentially. Ten to 20 images were acquired with a minimum of 3 biological replicates. Individual images were processed using ImageJ. A minimum of 10 regions of interest (ROIs) at PD (using AB as a marker) and in the surrounding PM were manually outlined, and the signal intensity was

calculated as the mean gray value (sum of gray values of all the pixels in the selected area divided by the ROI surface) for each ROI.

Immunolabeling of callose

The level of callose deposition was determined in leaves and in the pericarp of fruits harvested at 5 and 15 DPA. Leaf fragments were fixed with a 4% (v/v) formaldehyde solution in 1× PBS for 30 min, using vacuum infiltration (~100 kPa). They were then embedded in 6% (w/v) SeaKem LE agarose (Lonza, Basel, Switzerland), and sections of 100 μm were realized using a vibrating blade microtome (Microm 650 V; Thermo Fischer Scientific, Walldorf, Germany). Equatorial pericarp fragments were fixed using the same protocol. Pericarp sections of 80 or 150 μm were prepared, and fixed once more in fresh formaldehyde solution for 30 min, rinsed and kept in 1× PBS until use. The leaf and pericarp sections were then processed using the same protocol. The sections were deposited into a small basket containing MTSB buffer (50 mM PIPES, 5 mM EGTA, 5 mM MgSO_4 , pH = 7) to perform the immunolabeling of callose using the In Situ Pro VSi automated immunohistochemistry device from Intavis (Köln, Germany). Leaf and pericarp sections were rinsed 4 times for 10 min with 700 μL of MTSB. The sections were then incubated for 1 h with 700 μL of a 10% (v/v) DMSO/3% (v/v) IGEPAL CA-630 (Merck, Darmstadt, Germany) in MTSB. After rinsing, pericarp sections were incubated for 2 h in a 5% (v/v) Normal Donkey serum (NDS; Merck) blocking solution in MTSB, and 4 h with 700 μL of a 1/250 dilution of Anti-callose primary antibody (Biosupplies) in MTSB supplemented with 5% (v/v) NDS. The sections were then washed 6 times with 700 μL of MTSB, and incubated for 2 h with 700 μL of a 1/250 dilution of anti-mouse IgG Alexa Fluor 555 secondary antibody (ab150106; Abcam, Cambridge, UK) in MTSB + 5% (v/v) NDS. Sections were rinsed 6 times in MTSB and incubated with 1 $\mu\text{g}/\text{mL}$ Calcofluor white (Fluorescent Brightener 28 disodium salt solution, Merck, in MTSB). After rinsing, the sections were mounted on glass slides with Citifluor (AF1-25) (EMS Acquisition Corp., PA, USA) and the slides sealed with nail polish.

Imaging was performed using a Zeiss LSM 880 confocal microscope equipped with a Zeiss $\times 20$ dry objective (numerical aperture 0.8). For Alexa 555, excitation was performed at 561 nm with an argon laser (0.3% intensity) and fluorescence emission was collected at 570 to 630 nm by a GaAsP detector with 700 V gain. For Calcofluor imaging, excitation was performed at 405 nm (0.2% intensity) and fluorescence emission collected at 430 to 490 nm by a PMT with 700 V gain. Identical confocal microscope acquisition parameters were used for all the samples. Because of the highly heterogeneous cellular structure of pericarp and leaf, the total signal intensity of each tissue was quantified, and signal intensity values were measured by integrating the gray value of all the pixels above the same threshold. A minimum of 6 measurements was performed at least on 5 sections from at least 3 different fruits or leaves from different plants, and the experiment was repeated twice.

During the callose immunolabeling experiments, leaf thickness, cell perimeter in leaves or fruits have been manually measured following staining with Calcofluor on pictures acquired from confocal microscopy using ImageJ.

DANS assays

Before proceeding the DANS assay, 4-wk-old tomato plants were pretreated by spraying water (mock) or 10 mM H_2O_2 , followed by a 2 h incubation. Then 8 separated droplets (corresponding to 1 μL each) of 1 mM CFDA (Merck, Darmstadt, Germany) were loaded on the upper (adaxial) surface of a leaf. Then, the diffusion of the dye was monitored on the lower (abaxial) surface of the leaf, 5 min after loading CFDA, using an Axiozoom stereomicroscope V16 (Carl Zeiss Microscopy) equipped with a Zeiss Plan-Neofluar 0.5× (NA 0.19) objective lens, a fluorescence lamp (Lumencor Sola LED) and a GFP-BP filter cube (excitation 450/490 and emission 500/550). Several leaves with the same size were used from at least 4 to 5 plants ($n = 100$). Imaging was performed at the same magnification (28×), fluorescence lamp power (70%) and exposure time (750 ms). Images were acquired using a CMOS AxioCam 105 color camera. The CF signal intensity was measured on ImageJ by integrating the signal intensity to the pixel surface.

Co-immunoprecipitation and mass-spectrometry analysis

Total protein extracts from 100 mg of 35S::FW2.2-YFP fruit pericarp tissue were prepared using the following buffer: 1× PBS, cOMplete Protease Inhibitor Cocktail tablets (Roche, Mannheim, Germany), and 1% (v/v) Triton X-100. Samples were incubated in the extraction buffer at 4°C for 30 min with agitation, and then centrifuged (16,000 g, 10 min, 4°C). Prior to co-immunoprecipitation, western blotting was used to check the presence of the expressed tagged-FW2.2 protein in the supernatant (Supplementary Fig. S12). The supernatant containing the resuspended proteins was then used for immunoprecipitation assay using anti-GFP microbeads provided in the μMACS Epitope Tag Protein Isolation Kit according to the manufacturer's protocol (Miltenyi Biotec, Bergisch Gladbach, Germany). Approximately 500 μg of soluble proteins was loaded for each co-IP assay.

Fifty μL of the resulting eluate was loaded on a 10% (w/v) SDS-PAGE acrylamide gel; gel bands were manually cut and transferred to 1.5 mL Eppendorf tubes. Bands were first washed with 500 μL of water and then 500 μL of 25 mM NH_4HCO_3 . Destaining was performed twice in the presence of 500 μL of 50% (v/v) acetonitrile (ACN) in 25 mM NH_4HCO_3 . Gel bands were dehydrated twice by 500 μL of 100% (v/v) ACN, and finally dried at room temperature. Following destaining, proteins were reduced with 500 μL of 10 mM DTT at 56 °C for 45 min. The supernatant was then removed and proteins were alkylated with 500 μL of 55 mM iodoacetamide for 30 min. Gel bands were washed twice

with 500 μL of 50% (v/v) ACN in 25 mM NH_4HCO_3 , then dehydrated by 500 μL of 100% (v/v) CH_3CN , and finally dried at room temperature. Twenty μL of a trypsin solution (Sequencing Grade Modified Trypsin, Promega, Madison, USA), at a concentration of 0.0125 $\mu\text{g}/\mu\text{L}$ in 25 mM NH_4HCO_3 , was added to every gel region and gel bands were kept for 10 min on ice. Fifty μL of 25 mM NH_4HCO_3 was added, and the samples were kept for another 10 min at room temperature. The digestion was performed overnight at 37 °C; then peptides were extracted by addition 100 μL of 2% (v/v) formic acid (FA). Gel bands were extracted twice by addition of 200 μL of 80% (v/v) ACN and 2% FA. After solvent evaporation in a Speed-vac, peptides were resuspended in 10 μL of 2% (v/v) FA, then purified with a micro tip C18 (Zip-Tip C18 Millipore Corporation Billerica MA, USA). Peptides were eluted with a solution containing 2% (v/v) FA and 80% (v/v) ACN and dried until total evaporation. Peptides were resuspended in 7 μL 2% (v/v) FA before LC-MS/MS analysis.

The LC-MS/MS were performed using the Ultimate 3000 RSLC nano system (Thermo Fisher Scientific Inc., Waltham, MA, USA) interfaced online with a nano easy ion source and the Exploris 240 Plus Orbitrap mass spectrometer (Thermo Fisher Scientific Inc., Waltham, MA, USA). The samples were analyzed in Data Dependent Acquisition (DDA). The raw files were analyzed with MaxQuant version 2.0.3 using default settings. The files were searched against the *S. lycopersicum* genome (ITAG4.1_release January 2022 https://solgenomics.net/organism/solanum_lycopersicum/genome 34,689 entries) added with the FW2.2-YFP. Identified proteins were filtered according to the following criteria: at least 2 different trypsin peptides with at least 1 unique peptide, an *E*-value below 0.01, and a protein *E*-value smaller than 0.01 were required. Using the above criteria, the rate of false peptide sequence assignment and false protein identification was lower than 1%. Proteins were quantified by label-free method with MaxQuant software using unique and razor peptides intensities (Cox et al. 2014). Statistical analyses were carried out using RStudio package software. The protein intensity ratio and statistical tests were applied to identify the significant differences in the protein abundance. Hits were retained if they were quantified in at least 4 of the 5 replicates in at least 1 experiment. Proteins with a significant quantitative ratio ($P < 0.05$ or 0.01 with or without Benjamini–Hochberg correction) were considered as significantly upregulated and downregulated, respectively.

The mass spectrometry proteomics data have been deposited to the ProteomeXchange Consortium via the PRIDE (Perez-Riverol et al. 2022) partner repository with the data set identifier PXD045350.

Tools for the prediction of the FW2.2 structure and topology

The 3-dimensional structure of the full-length FW2.2 (Q9LKV7) was obtained from the AlphaFold Protein

Structure Database (<https://alphafold.ebi.ac.uk/>) (Jumper et al. 2021; Varadi et al. 2022). DeepTMHMM (<https://dtu.biolib.com/DeepTMHMM>) (Hallgren et al. 2022) was used to predict the presence of transmembrane helix in FW2.2. The PPM 3.0 Web Server (https://opm.phar.umich.edu/ppm_server3_cgopm) (Lomize et al. 2022) was used with default parameters and plasma membrane (plants) type to predict the topology and insertion of FW2.2 in the plasma membrane.

Phylogenetic analyses

The SiCaS protein sequences were first retrieved from NCBI Blast using Arabidopsis CaS sequences, and analyzed at NGPhylogeny.fr (Lemoine et al. 2019) using the following parameters: Muscle alignment, BMGE alignment curation, maximum likelihood analysis PhyML. Bootstrap values are located at each node and were calculated from 1,000 replicates.

Acknowledgments

Mass spectrometry experiments were carried out using the facilities of the Montpellier Proteomics Platform (PPM, MSPP site, BioCampus Montpellier), member of the Proteomics French Infrastructure (ProFI). The microscopy analyses were performed in the Bordeaux Imaging Center, a service unit of the CNRS-INSERM and Bordeaux University, member of the national infrastructure France Biolmaging. The help of Lysiane Brocard is acknowledged. We express our deepest thanks to Naïs Daviddi, Lucie Ehrhard, and Ulysse Tuquoi, for their technical help during their internship, and to Isabelle Atienza, Aurélie Honoré, and Valérie Rouyère, for taking care of the plant culture in the greenhouse.

Author contributions

N.B., F.G., E.B., N.G., and C.C. conceived the project and designed the research. A.B. and N.B. performed the research. V.R. performed the IP-MS/MS proteomics experiments. M.G. helped in the callose immunolabeling experiments using the InsituPro VSi automate. All authors analyzed and discussed the results. A.B., N.B., N.G., and C.C. wrote the manuscript with input from the other authors.

Supplementary data

The following materials are available in the online version of this article.

Supplementary Figure S1. Plasma membrane localization and 3D-structure prediction of the FW2.2 protein.

Supplementary Figure S2. Characterization of plants expressing FW2.2 fused to YFP.

Supplementary Figure S3. RT-qPCR analysis of FW2.2 expression in tomato plants.

Supplementary Figure S4. CRISPR/Cas9-induced mutations producing truncated versions of FW2.2 lacking the PLAC8 domain.

Supplementary Figure S5. DANS assays in tomato leaves.

Supplementary Figure S6. Callose deposition in leaves from 35S::FW2.2 and CR-*fw*2.2 plants.

Supplementary Figure S7. Callose deposition in fruit pericarp of 35S::FW2.2 and CR-*fw*2.2 plants compared to WT.

Supplementary Figure S8. Pericarp cell perimeter in the different transgenic lines.

Supplementary Figure S9. Characterization of *Callose Synthase* genes in tomato.

Supplementary Figure S10. *CalS* expression level in leaves and fruit from WT, 35S::FW2.2, and CR-FW2.2 lines.

Supplementary Figure S11. Allele swapping complementation assays.

Supplementary Figure S12. Western blot using anti-GFP antibodies on protein extracts from 10 DPA pericarps of WT and 35S::FW2.2-YFP fruits.

Supplementary Table S1. List of primers used for constructs and RT-qPCR analysis.

Supplementary Table S2. List of Gateway vectors used for constructs.

Supplementary Data Set 1. List of proteins identified as interactors of FW2.2/CNR.

Funding

This work was carried out with the financial support of the French Agence Nationale de la Recherche (grant no. ANR-20-CE20-0002), the GPR Bordeaux Plant Sciences in the framework of the IdEX Bordeaux University “Investments for the Future” program, and the French Ministère de l’Enseignement Supérieur et de la Recherche (PhD grant to A.B.). The microscopy analyses performed in the Bordeaux Imaging Center were supported by the French Agence Nationale de la Recherche (ANR-10-INBS-04).

Conflict of interest statement. None declared.

Data availability

The data underlying this article are available in the article and in its online supplementary material.

References

Alpert KB, Grandillo S, Tanksley SD. *Fw2.2*: a major QTL controlling fruit weight is common to both red- and green-fruited tomato species. *Theor Appl Genet.* 1995;**91**(6–7):994–1000. <https://doi.org/10.1007/BF00223911>

Amsbury S, Kirk P, Benitez-Alfonso Y. Emerging models on the regulation of intercellular transport by plasmodesmata-associated callose. *J Exp Bot.* 2018;**69**(1):105–115. <https://doi.org/10.1093/jxb/erx337>

Baldet P, Hernould M, Laporte F, Mounet F, Just D, Mouras A, Chevalier C, Rothan C. The expression of cell proliferation-related genes in early developing flower is affected by fruit load reduction in tomato plants. *J Exp Bot.* 2006;**57**(4):961–970. <https://doi.org/10.1093/jxb/erj082>

Bauchet A, Gévaudant F, Gonzalez N, Chevalier C. In search of the still unknown function of FW2.2/CELL NUMBER REGULATOR, a major regulator of fruit size in tomato. *J Exp Bot.* 2021;**72**(15):5300–5311. <https://doi.org/10.1093/jxb/erab207>

Bisbis B, Delmas F, Joubès J, Sicard A, Hernould M, Inzé D, Mouras A, Chevalier C. Cyclin-dependent kinase (CDK) inhibitors regulate the CDK-cyclin complex activities in endoreduplicating cells of developing tomato fruit. *J Biol Chem.* 2006;**281**(11):7374–7383. <https://doi.org/10.1074/jbc.M506587200>

Blanca J, Montero-Pau J, Sauvage C, Bauchet G, Illa E, Díez MJ, Francis D, Causse M, van der Knaap E, Cañizares J. Genomic variation in tomato, from wild ancestors to contemporary breeding accessions. *BMC Genomics.* 2015;**16**(1):257. <https://doi.org/10.1186/s12864-015-1444-1>

Bolte S, Talbot C, Boutte Y, Catrice O, Read ND, Satiat-Jeunemaitre B. FM-dyes as experimental probes for dissecting vesicle trafficking in living plant cells. *J Microsc.* 2004;**214**(2):159–173. <https://doi.org/10.1111/j.0022-2720.2004.01348.x>

Brandizzi F, Frangne N, Marc-Martin S, Hawes C, Neuhaus J-M, ParisN. The destination for single-pass membrane proteins is influenced markedly by the length of the hydrophobic domain. *Plant Cell.* 2002;**14**(5):1077–1092. <https://doi.org/10.1105/tpc.000620>

Brault ML, Petit JD, Immel F, Nicolas WJ, Glavier M, Brocard L, Gaston A, Fouché M, Hawkins TJ, Crowet JM, et al. Multiple C2 domains and transmembrane region proteins (MCTPs) tether membranes at plasmodesmata. *EMBO Rep.* 2019;**20**(8):e47182. <https://doi.org/10.15252/embr.201847182>

Chakrabarti M, Zhang N, Sauvage C, Muñoz S, Blanca J, Cañizares J, Díez MJ, Schneider R, Mazourek M, McClead J, et al. A cytochrome P450 regulates a domestication trait in cultivated tomato. *Proc Natl Acad Sci U S A.* 2013;**110**(42):17125–17130. <https://doi.org/10.1073/pnas.1307313110>

Chen XY, Kim JY. Callose synthesis in higher plants. *Plant Signal Behav.* 2009;**4**(6):489–492. <https://doi.org/10.4161/psb.4.6.8359>

Concordet J-P, Haeussler M. CRISPOR: intuitive guide selection for CRISPR/Cas9 genome editing experiments and screens. *Nucleic Acids Res.* 2018;**46**(W1):W242–W245. <https://doi.org/10.1093/nar/gky354>

Cong B, Liu J, Tanksley SD. Natural alleles at a tomato fruit size quantitative trait locus differ by heterochronic regulatory mutations. *Proc Natl Acad Sci U S A.* 2002;**99**(21):13606–13611. <https://doi.org/10.1073/pnas.172520999>

Cong B, Tanksley SD. FW2.2 and cell cycle control in developing tomato fruit: a possible example of gene co-option in the evolution of a novel organ. *Plant Mol Biol.* 2006;**62**(6):867–880. <https://doi.org/10.1007/s11103-006-9062-6>

Cox J, Hein MY, Luber CA, Paron I, Nagaraj N, Mann M. Accurate proteome-wide label-free quantification by delayed normalization and maximal peptide ratio extraction, termed MaxLFQ. *Mol Cell Proteomics.* 2014;**13**(9):2513–2526. <https://doi.org/10.1074/mcp.M113.031591>

Cui W, Lee J-Y. Arabidopsis callose synthases CalS1/8 regulate plasmodesmal permeability during stress. *Nat Plants.* 2016;**2**(5):16034. <https://doi.org/10.1038/nplants.2016.34>

Cui W, Wang X, Lee J-Y. Drop-ANd-See: a simple, real-time, and non-invasive technique for assaying plasmodesmal permeability. *Methods Mol Biol.* 2015;**1217**:149–156. https://doi.org/10.1007/978-1-4939-1523-1_10

Dahan Y, Rosenfeld R, Zadiranov V, Irihimovitch V. A proposed conserved role for an avocado FW2.2-like gene as a negative regulator of fruit cell division. *Planta.* 2010;**232**(3):663–676. <https://doi.org/10.1007/s00425-010-1200-3>

De Franceschi P, Stegmeir T, Cabrera A, van der Knaap E, Rosyara UR, Sebolt AM, Dondini L, Dirlwanger E, Quero-García J, Campoy JA, et al. Cell number regulator genes in Prunus provide candidate genes for the control of fruit size in sweet and sour cherry. *Mol Breed.* 2013;**32**(2):311–326. <https://doi.org/10.1007/s11032-013-9872-6>

Doganlar S, Frary A, Daunay M-C, Lester RN, Tanksley SD. Conservation of gene function in the Solanaceae as revealed by

- comparative mapping of domestication traits in Eggplant. *Genetics*. 2002;**161**(4):1713–1726. <https://doi.org/10.1093/genetics/161.4.1713>
- Frary A, Nesbitt TC, Frary A, Grandillo S, van der Knaap E, Cong B, Liu J, Meller J, Elber R, Alpert KB, et al.** *Fw2.2*: a quantitative trait locus key to the evolution of tomato fruit size. *Science*. 2000;**289**(5476):85–88. <https://doi.org/10.1126/science.289.5476.85>
- Galaviz-Hernandez C, Stagg C, de Ridder G, Tanaka TS, Ko MSH, Schlessinger D, Nagaraja R.** Plac8 and Plac9, novel placental-enriched genes identified through microarray analysis. *Gene*. 2003;**309**(2):81–89. [https://doi.org/10.1016/S0378-1119\(03\)00508-0](https://doi.org/10.1016/S0378-1119(03)00508-0)
- Gallagher KL, Sozzani R, Lee C-M.** Intercellular protein movement: deciphering the language of development. *Annu Rev Cell Dev Biol*. 2014;**30**(1):207–233. <https://doi.org/10.1146/annurev-cellbio-100913-012915>
- Gaudioso-Pedraza R, Beck M, Frances L, Kirk P, Ripodas C, Niebel A, Oldroyd GED, Benitez-Alfonso Y, de Carvalho-Niebel F.** Callose-regulated symplastic communication coordinates symbiotic root nodule development. *Curr Biol*. 2018;**28**(22):3562–3577.e6. <https://doi.org/10.1016/j.cub.2018.09.031>
- Grandillo S, Ku HM, Tanksley SD.** Identifying the loci responsible for natural variation in fruit size and shape in tomato. *Theor Appl Genet*. 1999;**99**(6):978–987. <https://doi.org/10.1007/s001220051405>
- Grisson MS, Kirk P, Brault ML, Wu XN, Schulze WX, Benitez-Alfonso Y, Immel F, Bayer EM.** Plasma membrane-associated receptor-like kinases relocalize to plasmodesmata in response to osmotic stress. *Plant Physiol*. 2019;**181**(1):142–160. <https://doi.org/10.1104/pp.19.00473>
- Guo M, Rupe MA, Dieter JA, Zou J, Spielbauer D, Duncan KE, Howard RJ, Hou Z, Simmons CR.** *Cell Number Regulator1* affects plant and organ size in maize: implications for crop yield enhancement and heterosis. *Plant Cell*. 2010;**22**(4):1057–1073. <https://doi.org/10.1105/tpc.109.073676>
- Hallgren, J., Tsirigos KD, Pedersen MD, Almagro Armenteros JJ, Marcatili P, Nielsen H, Krogh A, Winther O.** DeepTMHMM predicts alpha and beta transmembrane proteins using deep neural networks. *BioRxiv* 2022-04. <https://doi.org/10.1101/2022.04.08.487609>, 10 April 2022, preprint: not peer reviewed.
- Han X, Hyun TK, Zhang M, Kumar R, Koh E-J, Kang B-H, Lucas WJ, Kim J-Y.** Auxin-callose-mediated plasmodesmal gating is essential for tropic auxin gradient formation and signaling. *Dev Cell*. 2014a;**28**(2):132–146. <https://doi.org/10.1016/j.devcel.2013.12.008>
- Han X, Kumar D, Chen H, Wu S, Kim J-Y.** Transcription factor-mediated cell-to-cell signalling in plants. *J Exp Bot*. 2014b;**65**(7):1737–1749. <https://doi.org/10.1093/jxb/ert422>
- Jumper J, Evans R, Pritzel A, Green T, Figurnov M, Ronneberger O, Tunyasuvunakool K, Bates R, Židek A, Potapenko A, et al.** Highly accurate protein structure prediction with AlphaFold. *Nature*. 2021;**596**(7873):583–589. <https://doi.org/10.1038/s41586-021-03819-2>
- Lemoine F, Correia D, Lefort V, Doppelt-Azeroual O, Mareuil F, Cohen-Boulakia S, Gascuel O.** NGPhylogeny.fr: new generation phylogenetic services for non-specialists. *Nucleic Acids Res*. 2019;**47**(W1):W260–W265. <https://doi.org/10.1093/nar/gkz303>
- Li Z, He C.** *Physalis floridana* Cell Number Regulator1 encodes a cell membrane-anchored modulator of cell cycle and negatively controls fruit size. *J Exp Bot*. 2015;**66**(1):257–270. <https://doi.org/10.1093/jxb/eru415>
- Libault M, Zhang X-C, Govindarajulu M, Qiu J, Ong YT, Brechenmacher L, Berg RH, Hurlley-Sommer A, Taylor CG, Stacey G.** A member of the highly conserved FWL (tomato FW2.2-like) gene family is essential for soybean nodule organogenesis: a soybean FWL essential for nodulation. *Plant J*. 2010;**62**(5):852–864. <https://doi.org/10.1111/j.1365-3113.2010.04201.x>
- Lippman ZB, Tanksley SD.** Dissecting the genetic pathway to extreme fruit size in tomato using a cross between the small-fruited wild species *Lycopersicon pimpinellifolium* and *L. esculentum* var. *giant* heirloom. *Genetics*. 2001;**158**(1):413–422. <https://doi.org/10.1093/genetics/158.1.413>
- Liu J, Cong B, Tanksley SD.** Generation and analysis of an artificial gene dosage series in tomato to study the mechanisms by which the cloned quantitative trait locus fw2.2 controls fruit size. *Plant Physiol*. 2003;**132**(1):292–299. <https://doi.org/10.1104/pp.102.018143>
- Lomize AL, Todd SC, Pogozheva ID.** Spatial arrangement of proteins in planar and curved membranes by PPM 3.0. *Protein Sci*. 2022;**31**(1):209–220. <https://doi.org/10.1002/pro.4219>
- Marshall OJ.** PerlPrimer: cross-platform, graphical primer design for standard, bisulphite and real-time PCR. *Bioinformatics*. 2004;**20**(15):2471–2472. <https://doi.org/10.1093/bioinformatics/bth254>
- Martinière A, Lavagi I, Nageswaran G, Rolfe DJ, Maneta-Peyret L, Luu D-T, Botchway SW, Webb SED, Mongrand S, Maurel C, et al.** Cell wall constrains lateral diffusion of plant plasma-membrane proteins. *Proc Natl Acad Sci U S A*. 2012;**109**(31):12805–12810. <https://doi.org/10.1073/pnas.1202040109>
- Martinière A, Gibrat R, Sentenac H, Dumont X, Gaillard I, Paris N.** Uncovering pH at both sides of the root plasma membrane interface using noninvasive imaging. *Proc Natl Acad Sci U S A*. 2018;**115**(25):6488–6493. <https://doi.org/10.1073/pnas.1721769115>
- Maule AJ, Benitez-Alfonso Y, Faulkner C.** Plasmodesmata—membrane tunnels with attitude. *Curr Opin Plant Biol*. 2011;**14**(6):683–690. <https://doi.org/10.1016/j.pbi.2011.07.007>
- Mu Q, Huang Z, Chakrabarti M, Illa-Berenguer E, Liu X, Wang Y, Ramos A, van der Knaap E.** Fruit weight is controlled by cell size regulator encoding a novel protein that is expressed in maturing tomato fruits. *PLoS Genet*. 2017;**13**(8):e1006930. <https://doi.org/10.1371/journal.pgen.1006930>
- Nafati M, Cheniclet C, Hernould M, Do PT, Fernie A, Chevalier C, Gévaudant F.** The specific overexpression of a cyclin dependent kinase inhibitor in tomato fruit mesocarp cells uncouples endoreduplication and cell growth. *Plant J*. 2011;**65**(4):543–556. <https://doi.org/10.1111/j.1365-3113.2010.04446.x>
- Nesbitt TC, Tanksley SD.** *Fw2.2* directly affects the size of developing tomato fruit, with secondary effects on fruit number and photosynthate distribution. *Plant Physiol*. 2001;**127**(2):575–583. <https://doi.org/10.1104/pp.010087>
- O'Lexy R, Kasai K, Clark N, Fujiwara T, Sozzani R, Gallagher KL.** Exposure to heavy metal stress triggers changes in plasmodesmatal permeability via deposition and breakdown of callose. *J Exp Bot*. 2018;**69**(15):3715–3728. <https://doi.org/10.1093/jxb/ery171>
- Perez-Riverol Y, Bai J, Bandla C, Garcia-Seisdedos D, Hewapathirana S, Kamatchinathan S, Kundu DJ, Prakash A, Frericks-Zipper A, Eisenacher M, et al.** The PRIDE database resources in 2022: a hub for mass spectrometry-based proteomics evidences. *Nucleic Acids Res*. 2022;**50**(D1):D543–D552. <https://doi.org/10.1093/nar/gkab1038>
- Petit JD, Li ZP, Nicolas WJ, Grisson MS, Bayer EM.** Dare to change, the dynamics behind plasmodesmata-mediated cell-to-cell communication. *Curr Opin Plant Biol*. 2020;**53**:80–89. <https://doi.org/10.1016/j.pbi.2019.10.009>
- Platre MP, Satbhai SB, Brent L, Gleason MF, Cao M, Grisson M, Glavier M, Zhang L, Gaillochet C, Goeschl C, et al.** The receptor kinase SRF3 coordinates iron-level and flagellin dependent defense and growth responses in plants. *Nat Commun*. 2022;**13**(1):4445. <https://doi.org/10.1038/s41467-022-32167-6>
- Qiao Z, Brechenmacher L, Smith B, Strout GW, Mangin W, Taylor C, Russell SD, Stacey G, Libault M.** The Gm *FWL1* (*FW2-2-like*) nodulation gene encodes a plasma membrane microdomain-associated protein: a FW2-2-like protein is located in plasma membrane microdomains. *Plant Cell Environ*. 2017;**40**(8):1442–1455. <https://doi.org/10.1111/pce.12941>
- Ruan B, Shang L, Zhang B, Hu J, Wang Y, Lin H, Zhang A, Liu C, Peng Y, Zhu L, et al.** Natural variation in the promoter of *TGW2* determines grain width and weight in rice. *New Phytol*. 2020;**227**(2):629–640. <https://doi.org/10.1111/nph.16540>

- Saatian B, Kolhalmi SE, Cui Y.** Localization of Arabidopsis glucan synthase-like 5, 8, and 12 to plasmodesmata and the GSL8-dependent role of PDLP5 in regulating plasmodesmal permeability. *Plant Signaling Behav.* 2023;**18**(1):e2164670. <https://doi.org/10.1080/15592324.2022.2164670>
- Song W-Y, Martinoia E, Lee J, Kim D, Kim D-Y, Vogt E, Shim D, Choi KS, Hwang I, Lee Y.** A novel family of Cys-rich membrane proteins mediates cadmium resistance in Arabidopsis. *Plant Physiol.* 2004;**135**(2):1027–1039. <https://doi.org/10.1104/pp.103.037739>
- Song W-Y, Choi KS, Kim DY, Geisler M, Park J, Vincenzetti V, Schellenberg M, Kim SH, Lim YP, Noh EW, et al.** Arabidopsis PCR2 is a zinc exporter involved in both zinc extrusion and long-distance zinc transport. *Plant Cell.* 2010;**22**(7):2237–2252. <https://doi.org/10.1105/tpc.109.070185>
- Song L, Wang R, Zhang L, Wang Y, Yao S.** CRR1 encoding callose synthase functions in ovary expansion by affecting vascular cell patterning in rice. *Plant J.* 2016;**88**(4):620–632. <https://doi.org/10.1111/tpj.13287>
- Swinnen G, Mauxion J-P, Baekelandt A, De Clercq R, Van Doorselaere J, Inzé D, Gonzalez N, Goossens A, Pauwels L.** SLKX8 and SLKX9 are negative regulators of leaf and fruit growth in tomato. *Plant Physiol.* 2022;**188**(1):382–396. <https://doi.org/10.1093/plphys/kiab464>
- Tee EE, Johnston MG, Papp D, Faulkner C.** A PDLP-NHL3 complex integrates plasmodesmal immune signaling cascades. *Proc Natl Acad Sci U S A.* 2023;**120**(17):e2216397120. <https://doi.org/10.1073/pnas.2216397120>
- Thomas CL, Bayer EM, Ritzenthaler C, Fernandez-Calvino L, Maule AJ.** Specific targeting of a plasmodesmal protein affecting cell-to-cell communication. *PLoS Biol.* 2008;**6**(1):e7. <https://doi.org/10.1371/journal.pbio.0060007>
- Tourdot E, Mauxion J-P, Gonzalez N, Chevalier C.** Endoreduplication in plant organogenesis: a means to boost fruit growth. *J Exp Bot.* 2023;**74**(20):6269–6284. <https://doi.org/10.1093/jxb/erad235>
- Usak D, Haluska S, Pleskot R.** Callose synthesis at the center point of plant development—an evolutionary insight. *Plant Physiol.* 2023;**193**(1):54–69. <https://doi.org/10.1093/plphys/kiad274>
- van der Knaap E, Tanksley SD.** The making of a bell pepper-shaped tomato fruit: identification of loci controlling fruit morphology in Yellow Stuffer tomato. *Theor Appl Genet.* 2003;**107**(1):139–147. <https://doi.org/10.1007/s00122-003-1224-1>
- Van Norman JM, Breakfield NW, Benfey PN.** Intercellular communication during plant development. *Plant Cell.* 2011;**23**(3):855–864. <https://doi.org/10.1105/tpc.111.082982>
- Varadi M, Anyango S, Deshpande M, Nair S, Natassia C, Yordanova G, Yuan D, Stroe O, Wood G, Laydon A, et al.** AlphaFold Protein Structure Database: massively expanding the structural coverage of protein-sequence space with high-accuracy models. *Nucl Acids Res.* 2022;**50**(D1):439–444. <https://doi.org/10.1093/nar/gkab1061>
- Wang Y, Perez-Sancho J, Platre MP, Callebaut B, Smokvarska M, Ferrer K, Luo Y, Nolan TM, Sato T, Busch W, et al.** Plasmodesmata mediate cell-to-cell transport of brassinosteroid hormones. *Nat Chem Biol.* 2023;**19**(11):1331–1341. <https://doi.org/10.1038/s41589-023-01346-x>
- Weber E, Gruetzner R, Werner S, Engler C, Marillonnet S.** Assembly of designer TAL effectors by Golden Gate cloning. *PLoS One.* 2011;**6**(5):e19722. <https://doi.org/10.1371/journal.pone.0019722>
- Wei Z, Wang J, Yang S, Song Y.** Identification and expression analysis of the LRR-RLK gene family in tomato (*Solanum lycopersicum*) Heinz 1706. *Genome.* 2015;**58**(4):121–134. <https://doi.org/10.1139/gen-2015-0035>
- Weinl C, Marquardt S, Kuijt SJH, Nowack MK, Jakoby MJ, Hülskamp M, Schnittger A.** Novel functions of plant cyclin-dependent kinase inhibitors, ICK1/KRP1, can act non-cell-autonomously and inhibit entry into mitosis. *Plant Cell.* 2005;**17**(6):1704–1722. <https://doi.org/10.1105/tpc.104.030486>
- Wu S, Gallagher KL.** Mobile protein signals in plant development. *Curr Opin Plant Biol.* 2011;**14**(5):563–570. <https://doi.org/10.1016/j.pbi.2011.06.006>
- Wu S-W, Kumar R, Iswanto ABB, Kim J-Y.** Callose balancing at plasmodesmata. *J Exp Bot.* 2018;**69**(22):5325–5339. <https://doi.org/10.1093/jxb/ery317>
- Xu J, Xiong W, Cao B, Yan T, Luo T, Fan T, Luo M.** Molecular characterization and functional analysis of “fruit-weight2.2-like” gene family in rice. *Planta.* 2013;**238**(4):643–655. <https://doi.org/10.1007/s00425-013-1916-y>
- Yan D, Yadav SR, Paterlini A, Nicolas WJ, Petit JD, Brocard L, Belevich I, Grison MS, Vaten A, Karami L, et al.** Sphingolipid biosynthesis modulates plasmodesmal ultrastructure and phloem unloading. *Nat Plants.* 2019;**5**(6):604–615. <https://doi.org/10.1038/s41477-019-0429-5>
- Zsögön A, Čermák T, Naves ER, Notini MM, Edel KH, Weinl S, Freschi L, Voytas DF, Kudla J, Peres LEP.** De novo domestication of wild tomato using genome editing. *Nat Biotechnol.* 2018;**36**(12):1211–1216. <https://doi.org/10.1038/nbt.4272>